Journal of Marine Research, 46, 215–265, 1988

Journal of
MARINE RESEARCH

Volume 46, Number 2

Buoyancy driven planetary flows

by A. Colin de Verdière[1]

ABSTRACT

The large scale flow patterns driven by surface buoyancy flux are obtained as numerical solutions of the planetary geostrophic equations to which dissipation and diffusion have been appended. Within a cartesian β plane, square box geometry, the solution is made of gyres of the largest possible size with western and northern intensification, anticyclonic above the main thermocline, cyclonic below. Within regions of heat gain, the classical equilibrium between downward eddy diffusion and vertical upwelling is approximately observed in the main thermocline. As a consequence the abyssal circulation (southern interior and western boundary current) behave according to the early Stommel-Arons' ideas. The situation is rather different in regions of heat losses where convection is active: the flow patterns consist of swift zonal flows with horizontal divergence whose dynamics involve lateral diffusion of density and vorticity. The solutions are mostly sensitive to the choice of the vertical diffusion coefficient whose value between 1 and 2 $cm^2\ s^{-1}$ produces realistic bottom water formation rates and meridional heat fluxes. The bulk of the heat accumulated in the Tropics is transported poleward by a direct Hadley cell (northward at the surface, southward at depth) obtained through a zonal averaging of the meridional circulation: horizontal rotational recirculations are less important for the heat transport.

1. Introduction

Air-sea heat exchange maps at the ocean surface show the pattern of buoyancy forcing to which the circulation must respond in order to keep the ocean in steady state. Negative anomalies of several tens of watts $\cdot\ m^{-2}$ near western boundaries reflect the characteristics of the surface oceanic flow and not that of the atmosphere. Balancing the surface buoyancy flux by vertical advection in the upper few hundred meters of water yields vertical velocities fully comparable with Ekman pumping through which

1. IFREMER, B. P. 337, Brest 29273, France.

generations of wind-driven models have been forced, revealing the importance of this concurrent oceanic forcing. The consideration of large scale buoyancy forcing has proceeded in the past along two directions: thermocline theories whose objective is to explain the presence of the oceanic main thermocline (see Veronis (1969) for a review) given a limited set of boundary conditions on the one hand, and abyssal circulation theories on the other: Stommel and Arons (1960) had the far-reaching idea of reconstructing abyssal planetary flow patterns given simple distributions of sources and sinks of *mass* at some intermediate levels near the base of the main thermocline. This idea bypassed the inherent difficulties of determining both the stratification and the circulation of a mid latitude oceanic basin. The mass distribution chosen (i.e., sinking in narrow places and uniform upwelling in the interior) was made plausible by the idea that the upwelling of cold water balances the heat input from the atmosphere over large regions. The success of the idea was of course the prediction of a deep western boundary current flowing equatorward (away from the polar sinking regions) accompanied by an important horizontal recirculation. Such boundary currents were actually found while the slow interior poleward recirculation remains unchecked. Of course, Stommel-Arons' constructions fall short of calculating the important meridional oceanic heat transport that must take place on account of the north-south differential heating mentioned above.

General oceanic circulation models (Bryan and Cox, 1968) based on the primitive equations incorporating rather complete dynamics from the rapid inertial gravity waves to the basin-wide slow moving gyres have addressed the full coupled problem of determining both the thermal and mass field. Being expensive to run, their applications have been oriented toward more realistic geometry and complex combined buoyancy and wind-driven forcing focusing on description of vigorous upper thermocline flows (Bryan and Cox, 1984) or global climate modelling (Bryan *et al.*, 1974).

Clearly the need exists for models simpler in geometry, forcing and dynamics than the present GCMs, to explore the validity of Stommel-Arons' ideas, to show the contribution of horizontal planetary flow patterns in the meridional heat transport and finally to assess the sensitivity of the solutions to parameterizations of unresolved processes. The present study offers such an approach using a model built around "reduced," filtered equations adapted for the slow time scale of oceanic response to buoyancy driving. The quasigeostrophic system is an example of a reduced system which filters out the inertia-gravity waves. It cannot be used here however because the requirement that the excursions of isopycnals around some *given* background stratification be small is far too severe for planetary scale buoyancy driven flow. The planetary geostrophic system described below is a far better choice: it is known as the Burger's system in the meteorological literature (Phillips, 1963), and as the "thermocline equations" in the oceanographic context, (Robinson and Stommel, 1959). The advantage of this formulation for the ocean was noticed by Charney in a discussion about numerical ocean models (1975) on account of the 4 octaves of scale separation

between the internal Rossby radius of deformation (50 km) and the general circulation scales (1000 km). (The situation is far less favorable in the atmosphere with a synoptic scale at 1000 km closer to the scale of the quasipermanent centers of action.) In such a system the inertial terms in the momentum equations are neglected altogether. Such a sweeping approximation filters out both inertia-gravity waves and dispersive Rossby waves and tunes the model to the long time scales appropriate to buoyancy forcing. There is no doubt that this approximation is a good first step in the interior of the ocean but a problematic one at western boundaries near which *permanent* return flows have cross-stream scales comparable to the internal Rossby radius. Because of this strong western boundary nonlinearity and the possible ensuing instabilities, the interior response could be completely modified. Nevertheless simpler problems which neglect this aspect are probably useful. The western boundary currents found herein are an order of magnitude broader than in nature; while their volume transports are realistic, the velocities are not.

This paper has been organized as follows: Section 2 presents the physics of the planetary geostrophic model (PG in what follows), most of the numerical details being deferred to an Appendix. The spin-up of a "typical" buoyancy driven solution is found in Section 3 and the energetics of the steady state in Section 4, while Section 5 describes the basic features of a chosen steady state solution as revealed by the various fields of pressure, density, velocity and potential vorticity. Section 6 presents the main results of this paper: the varieties of heat and vorticity regimes and the relevance of Stommel-Arons' idea to the observed flow patterns. Different perspectives are provided by the zonally averaged circulations which are discussed along with the meridional heat transport in Section 7. Some curious solutions with zonal asymmetry have been obtained on the f-plane. They are compared with the previous β plane results in Section 8. The small amplitude limit in Section 9 allows to identify those features of the solution which have a nonlinear origin. The paper concludes with Section 10 which offers a short parameter sensitivity study testing the robustness of the previous solution.

2. The model

For time scales much in excess of a pendulum day and horizontal scales of the order of the Earth radius, therefore large compared to the internal Rossby radius, scaling shows that motion in a thin layer of stratified fluid on a rotating earth obeys:

$$\begin{aligned} f\mathbf{k}x\mathbf{u} &= -\nabla P/\rho_o \\ -P_z - g\rho &= 0 \\ \nabla \cdot \mathbf{u} &= 0 \\ \frac{D\rho}{Dt} &= 0 \end{aligned} \tag{1}$$

where **k** is a vertical unit vector, $f = 2\Omega\sin\theta$ is the Coriolis parameter and θ is the latitude. The idea of using this planetary geostrophic set to construct numerical models of the general circulation is not new: it is the basis for the Hamburg climate model, (Hasselman, 1982). The great benefit is that fast time scale waves are filtered out, the only remaining wave mode being the slow nondispersive baroclinic Rossby wave. Such limits have been discussed by Phillips (1963) and more recently by Gent and McWilliams (1983) who show that the PG set has leading order accuracy when $\gamma = \beta L/f_o$ is order 1 and the Burger number $B = N^2H^2/f^2L^2$ is of order Rossby number. To obtain accuracy of the order of the Rossby number given these scales of motions would require solving the full primitive equations. Colin de Verdière (1986) investigated baroclinic instability within the inviscid set showing that baroclinic instability is not only possible but occurs with unbounded growth rates. Ad-hoc dissipation is necessary to bound the growth rate and render the problem well posed. In a continuously forced system it is also required to obtain steady solutions in a closed basin. Salmon (1986) has used a simple linear drag law in a recent linear analytical solution. Correct implementation of slip boundary conditions at vertical boundaries with such a choice of dissipation requires a transformation of system (1) to a single partial differential equation for pressure with nonclassical boundary conditions on pressure. There are two reasons why a Laplacian friction law has been preferred here: first, friction can be minimized at the large scale with such a scale-dependent operator and second, it was thought easier to work directly with the set (1) (with friction terms added). Of course no-slip boundary conditions must now be appended. With such Laplacian operators in the momentum equations one cannot solve analytically for velocities knowing the pressure gradient: a coupled system of two Helmholtz equations must be solved numerically. The implementation of vertical and lateral mixing for density is straightforward in this nonisopycnal model. In situations of static instability, a nonpenetrative convective adjustment is also used which restores the density to a neutral profile conserving the vertically integrated density content. In the present study, the fluid is assumed to have only one active component, temperature, and the simplest equation of state is used:

$$\rho = \rho_o(1 - \alpha(T - T_o))$$

It remains to specify the forcing: a mixed layer of constant depth is assumed, the windstress being distributed as a constant body force over it. When the cooling is such that the density profile of the mixed layer becomes unstable, only the density is mixed down; the stress remains at the top. Again simple specification of thermal forcing is used. A zonally uniform atmosphere prescribes atmospheric temperature and the surface heat flux obeys a Newtonian law as in Haney (1971), being proportional to the temperature difference between surface temperature and atmospheric temperature. Heat is exchanged to lower depths via explicit vertical mixing and (or) convective

adjustment mentioned previously. The forced-dissipative set to be solved is therefore:

$$\begin{aligned} f\mathbf{k}x\mathbf{u} &= -\nabla P/\rho_o + A\nabla^2\mathbf{u} + \tau/(\rho_o H_M)Y(Z) \\ -P_z - g\rho &= 0 \\ \nabla \cdot \mathbf{u} &= 0 \\ \frac{D\rho}{Dt} &= K(\rho_a - \rho)Y(Z) + K_v\rho_{zz} + K_H\nabla^2\rho + C_o \end{aligned} \tag{2}$$

in which $Y(Z)$ ($=1$ for $-H_M \le Z \le 0$ and zero elsewhere) specifies the mixed layer of depth H_M · C_o is the term representing nonpenetrative convective adjustment and as such it cannot be parameterized explicitly. It is subject to the constraint

$$\int_{-H}^{0} C_o\, dz = 0$$

as heat is only redistributed internally. These equations are to be solved with the boundary conditions that the total horizontal velocity and normal density flux vanish at solid boundaries. Note that the hydrostatic assumption is used everywhere implying that the vertical flow slips along the vertical boundaries. This is another departure from Salmon's (1986) study.

There remains the choice of geometry. A proper method to obtain solutions at planetary scale should use a spherical geometry. As very little is known about the numerical properties of the PG system, the basic ideas are explored here within a Cartesian geometry; i.e., a β plane. It is of course expected that the solutions should differ quantitatively in the two geometries but it is felt that an examination of the "regional physics" of the solutions should be qualitatively similar.

The corresponding vorticity and divergence equations derived from (2) are:

$$-A\nabla^2\xi + \beta v = fw_z \tag{3}$$

$$f\xi - \beta u = \frac{\nabla^2 P}{\rho_o} + A\nabla^2 w_z \tag{4}$$

where ξ is the vertical component of the relative vorticity vector. Eq. (3) shows that the model is dominated by the widely used planetary vorticity balance provided that the dissipation of vorticity is not too large. This dissipation of vorticity occurs mostly in boundary currents and for a given resolution the friction coefficient A is chosen so that frictionally driven boundary currents are correctly resolved.

It is possible to transform (3) and (4) by introducing the streamfunction Ψ and the velocity potential χ to decompose the horizontal velocity as:

$$\mathbf{u} = \mathbf{k}x\nabla\Psi + \nabla\chi.$$

The result is:

$$A\nabla^4\Psi + J(f, \Psi) + \nabla \cdot (f\nabla\chi) = 0 \tag{5}$$

$$A\nabla^4\chi + J(f, \chi) + \nabla \cdot (f\nabla\Psi) = \frac{\nabla^2 P}{\rho_o}. \tag{6}$$

In this planetary limit the pressure is not a streamfunction and as the symmetry of the equations shows, the divergent part of the flow is comparable with the rotational part. This is one of the main difference with quasigeostrophy along with the consideration of the full density equation.

It is now useful to present the appropriate energy equation for the forced-dissipative system (2). Such an energy conservation law includes only potential energy, the sole contributor at scales large compared to the Rossby radius. To derive it, multiply the horizontal momentum equations by **u**, the density equation by $g(z - z_R)$ (where z_R is an arbitrary reference depth), add them, and integrate over the volume of the domain of interest (with constant depth) using the boundary conditions, the end result being:

$$\frac{\partial}{\partial t}\iiint \rho g(z - z_r)\, dv = KgH_M(z_R - H_M/2)\iint[\rho_a - \rho(0)]\, ds + gK_v\iint[\rho(-H) - \rho(0)]\, ds + \iiint gc_o(z - z_R)\, dv + \iint \mathbf{u}(0)\tau/\rho_o\, ds - A\iiint |\nabla u|^2 + |\nabla v|^2\, dv \tag{7}$$

in which dv and ds represent the volume and horizontal surface element of integration respectively. Potential energy changes are successively contributed by:

(1) The net buoyancy forcing at the surface: in a steady state solution this term must vanish.

(2) The vertical mixing: note that this term is always positive reflecting the fact that vertical mixing raises the center of gravity of the fluid.

(3) The convective mixing in statistically unstable situations: it is negative as it forces heavy (light) fluid down (up).

(4) The rate of work of the wind stress at the ocean surface, a positive term.

(5) The dissipation by lateral friction.

In the numerical model developed here the energy equation plays a central role and the discretization of the equations has been chosen to preserve the energetics of the continuous system.

The method for solving equations (2) is based on a decomposition of the system in the vertical baroclinic and barotropic modes, a separation with powerful consequences when nonlinearity in the momentum equations and topographic variations of the ocean floor are absent. The horizontal velocity **u** is written as the sum of a barotropic

component $\mathbf{u}^+$ and baroclinic component $\mathbf{u}^-$: $\mathbf{u} = \mathbf{u}^+ + \mathbf{u}^-$ where

$$\int_{-H}^{0} \mathbf{u}^- \, dz = 0.$$

After a vertical integration of the continuity and momentum equations in (2) and imposing zero vertical velocity at both the ocean surface and the bottom, one obtains:

$$\nabla_H \cdot \mathbf{u}^+ = 0 \tag{8a}$$

$$f\mathbf{k} \times \mathbf{u}^+ = -\nabla\langle P\rangle/\rho_o + A\nabla^2 \mathbf{u}^+ + \tau/\rho_o H \tag{8b}$$

where the brackets $\langle\,\rangle$ represent the vertical average operation

$$H^{-1} \int_{-H}^{0} (\,)\, dz$$

and ∇_H the horizontal divergence operator. The set (8) defines completely the barotropic mode: it is horizontally nondivergent and *time independent*. At this level of approximation dispersive barotropic Rossby waves are filtered out and the barotropic mode responds instantaneously to forcing. Taking the curl of (8b) and introducing a streamfunction Ψ^+ gives:

$$-A\nabla^4 \Psi^+ + \beta\Psi_x^+ = \nabla \times \tau/\rho_o H \tag{9}$$

with $\Psi^+ = \partial\Psi^+/\partial n = 0$ at boundaries. The barotropic mode is entirely rotational and is the solution of Munk's problem. Subtracting out Eqs. (8) from (2) yields the set obeyed by the baroclinic mode:

$$\begin{aligned} f\mathbf{k} \times \mathbf{u}^- &= -\nabla(P - \langle P\rangle)/\rho_o + A\nabla^2\mathbf{u}^- + \tau/\rho_o(Y(z)H_M^{-1} - H^{-1}) \\ \nabla_H \cdot \mathbf{u}^- + w_z &= 0 \\ -P_z - g\rho &= 0 \\ \partial\rho/\partial t + (\mathbf{u}^+ + \mathbf{u}^-)_H \cdot \nabla\rho + w\rho_z &= K(\rho_a - \rho)Y(z) + K_v\rho_{zz} + K_H\nabla^2\rho. \end{aligned} \tag{10}$$

The barotropic mode can be solved independently of the baroclinic mode using Eq. (9). The sole interaction term in the baroclinic set (10) is the advection of the density field by the barotropic mode. In (10) only one variable, the density, is prognostic and initial states are therefore entirely determined by its specification. The method of solution follows: given ρ at time t, hydrostatic balance is first used to compute the pressure, the constant of integration being determined by the requirement that the vertical integral of pressure must vanish. Knowing the horizontal pressure gradient, it is then necessary to invert for horizontal velocities using the two momentum equations. This step is critical because the two coupled Helmhotz type equations must be solved in a situation in which the friction coefficient is small; i.e., a classical singular problem. Knowing the horizontal velocities, the divergence equation is integrated to obtain w. It is then possible to compute the advection terms and to advance the density forward in time

Table 1.

Number of grid points zonal, meridional, vertical	Ocean width L(km)	Ocean depth H(m)	A(cm^{2}s^{-1})	K_H(cm^{2}s^{-1})	K_v(cm^{2}s^{-1})	Time step (days)
LR 20 × 16 × 8	6000	4000	$6\ 10^9$	$2.5\ 10^6$–$5\ 10^7$	0.25–10	7.
HR 32 × 26 × 8	6000	4000	$1.45\ 10^9$	$7\ 10^6$	1.	3.5

using the density equation. Standard finite difference methods are used to discretize (9) and (10). Each variable is carried at each grid point in the horizontal while a staggered grid is used in the vertical, with w velocities computed at levels intermediate between those carrying horizontal velocity, density and pressure. The Appendix details the numerics and the computing aspects; suffice it to say here that the numerical scheme preserves potential energy conservation as in (7) and possesses two invariants, the first and second moment of the density, in the adiabatic limit.

This paper is concerned with strictly buoyancy-driven circulations, the wind-driven case being deferred to a later paper. This choice is made on purpose for the literature abounds in wind-driven simulations while much less has been said on the buoyancy-driven case. In this instance, the circulation is internal because the barotropic mode is not excited. Table 1 summarizes the simulations which have been carried out and the range of parameters explored. The geometry is that of rectangular ocean 6,000 km (4,800 km) in the zonal (meridional) direction. The flows are calculated on a constant β plane centered at 40° latitude so that the meridional extent of the model goes from about 20° to 60° of latitude. With the linear equation of state at hand, a linear distribution of atmospheric temperature is chosen as a function of y only varying from 25°C at the southern boundary to 2°C at the northern boundary. A constant heat exchange coefficient $Q_2 = 40\text{W m}^{-2}\text{°C}^{-1}$ has been selected within the range recommended by Haney (1971). The coefficient K present in the forcing term in (10) is then $Q_2/\rho_o C_p H_M$ where H_M is the mixed layer depth (=100 m in the present simulations) and C_p the heat capacity of water (=4500 J °C^{-1} Kg^{-1}). The equivalent time scale K^{-1} for the surface oceanic temperature to relax to the prescribed atmospheric temperature is then around 4 months.

The choice of resolution and of dissipative coefficients in Table 1 requires some discussion. The objective of the model is to obtain flow solutions whose interior dynamics are governed by the balance between planetary advection and vortex stretching, the last two terms in the vorticity equation (3). The frictional terms necessary to satisfy no slip boundary conditions become important on a lateral scale $\delta_M = (A/\beta)^{1/3}$ which is Munk's original boundary layer width. Within the model assumptions, horizontal resolution Δx must also be large compared to an oceanic internal Rossby radius. Insuring that several grid points span Munk's boundary layer is the main criterion used here to choose the friction coefficient A. It was found

empirically that a numerically correct representation of the model boundary current required:

$$A = 1.6\,\beta(\Delta x)^3.$$

The implied values of A are of course huge to mix the horizontal momentum at this resolution. The actual western boundary currents are smeared out in the present model and only transport values can be compared with field data. Although the friction coefficient is large, interior flows of scale L are geostrophic to order A/fL^2, a horizontal Ekman number which is the ratio of friction terms to Coriolis terms. For L of order 1000 km, this is less than 1% for the values used here. Of course the vertical divergence w_z may exceed the assumed interior value $\beta V/f$, a situation frequently observed in the model when baroclinic zonal flows impinge on meridional boundaries. In this instance the horizontal velocity and vertical vorticity vary on scales shorter than δ_M in order that vorticity diffusion equilibrates the larger stretching. Such boundary layers are not resolved here and it will be the purpose of comparisons between eddy resolving models and the present one to assess the importance of that issue.

The choices of the diffusion coefficients cannot be made independently of the lateral friction coefficient for a flow in thermal wind balance. The simplest way to see the connection is to eliminate w between (3) and the steady state density equation in (2) to obtain:

$$+A\nabla^2\xi + fK_H\,\partial/\partial_z[\nabla^2\rho/\rho_z] + fK_v\,\partial/\partial_z[\rho_{zz}/\rho_z] + f\,\partial/\partial_z[Co/\rho_z] = \beta v + f\,\partial/\partial_z[u_H\nabla\rho/\rho_z]. \quad (11)$$

Among the four nonconservative processes on the left-hand side the value of the first is already determined, the fourth one (convection) cannot be imposed but is a natural consequence of the model solutions. The influence of the second and third terms has to be minimized so that in statically stable regions the two terms on the right-hand side expressing the conservation of potential vorticity $f\rho_z$ become of leading order. In order that the diffusive terms do not exceed the order of the friction terms in the interior, geostrophic scaling of (11) shows that:

$$K_H/BA \leq 0\,(1) \text{ and } (L/\delta_M)^3\,K_v/WH \leq 0\,(1)$$

in which B is the Burger number N^2H^2/f^2L^2 previously mentioned. Taking $A = 3\ 10^9$ cm^2 s^{-1}, $L = 1000$ km, $H = 1000$ m, $W = 5\ 10^{-4}$ cm s^{-1} and $N = 5\ 10^{-3}$ s^{-1}, the above shows that K_H must be less than $7.5\ 10^6$ cm^2 s^{-1} and K_v less than 0.80 cm^2 s^{-1}. Such values within the observational range are used as pivots around which other regimes are explored. Vertical resolution is a direct consequence of the value of K_v: with centered differencing, a coarse vertical resolution leads to an instability noted by Bryan *et al.* (1974) in which density heavier than surface values may occur. When this is so, the present model fails to reach steady state. A choice of 8 levels guarantees that this does not happen except for the lowest value of the range of K_v in Table 1.

3. The spin-up

Once the stratification is initialized with mean temperature values characteristic of the North Atlantic the buoyancy forcing is switched on impulsively. The simulation named HR in Table 1 has been used to look at the establishment of the circulation. Kinetic and potential energies reveal three time scales of interest: initially both increase steadily for about 10 years at which time the kinetic energy reaches a maximum. This is followed by a 0 (100 years) adjustment at the end of which the important patterns are well established. The final period occurs on a very slow 0 (5,000 years) time scale, usually not well resolved by the present experiments of 800 years duration (exceptionally 1,200 years). This final period corresponds to the slow thermal adjustment of the deep temperature field while the motion fields are already spun up.

Characteristic x-t and y-t diagrams have been obtained for the first 100 years. Figure 1 shows two zonal cuts of the pressure field in subtropical and subpolar regions at level 2 (225 m). At southern latitudes the familiar westward propagation is evident: a baroclinic Rossby wave front starts from the east and moves westward at about 2.5 cm s^{-1}, crossing the ocean in about 10 years. The western boundary current is established on that Rossby wave time scale. Two time series of v and w at upper levels (Fig. 2) show some more details: initially the meridional velocity increases while w decreases, this tendency reversing at the passage of the front. This is associated with the westward displacement of a warm, anticyclonic pool above the main thermocline and the negative correlation between v and w is just what is needed to conserve potential vorticity. (A positive correlation occurs at lower levels as it should in a first baroclinic mode.) At northern latitudes, westward propagation is more elusive. As convection erodes the initial stratification the Rossby wave speeds are less. Furthermore eastward zonal flows are expected to oppose the wave front propagation. At deeper levels the adjustments are similar. A feature which emerges on that same time scale at the base of the main thermocline and in the deep water is an eastern boundary current in the northern part of the basin. On scales longer than the Rossby time scale, the adjustment is more gradual and uniform in the interior. This uniformity suggests that vertical mixing is the prime agent to bring the fields closer to equilibrium. In the subtropical gyre the positive vertical velocity induced by vertical mixing is the main agent to stop the westward propagation of the Rossby wave: a balance develops between southward planetary advection and compression of fluid columns by the upwelling above the main thermocline (see Section 6). Evidence of the second baroclinic Rossby mode is scant because its time scales are fully comparable with these mixing time scales.

The picture of adjustment provided by meridional characteristic diagrams adds some other aspects (Fig. 3). On such an eastern section, the northern part is spun up quickly and uniformly: after about 10 years steady state is obtained for both isotherms and isobars. This is the result of convection which occurs very efficiently for the first 5 years. The southern $\frac{2}{3}$ of the basin is subject to a far slower adjustment. A warm high

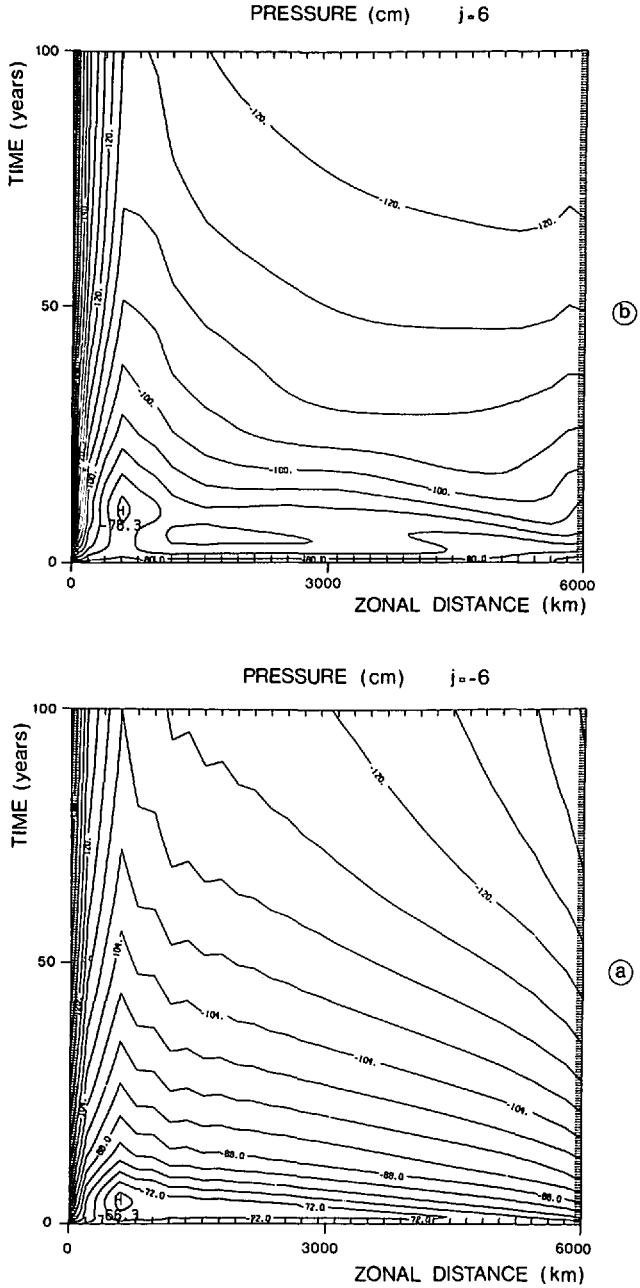

Figure 1. Pressure contours (cm) in characteristic $x-t$ diagrams at 225 m. Zonal cuts are given at subtropical (a) and subpolar latitudes (b) and run for the first 100 years.

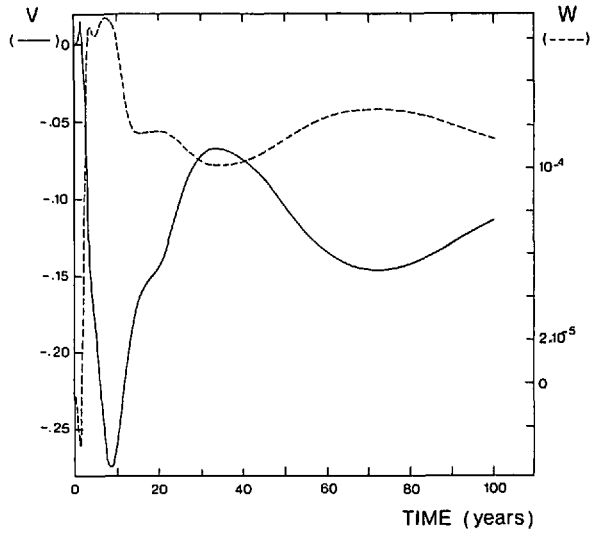

Figure 2. 100-year time series of meridional velocity and vertical velocity (dashed) at a location in the southeast quadrant of the model at 800 m. The negative correlation is a sign of the planetary vorticity balance. Units are in cm s^{-1}

pressure is quickly established above the main thermocline but it takes again of the order of a century for these shallow fields to get steady. At deeper levels, the quickly adjusted northern region shrinks in size and the southern pressure field evolves similarly to those above. The bulk of the motion fields (including the deep ones) are determined by thermodynamical processes occurring in and above the main thermocline and are established on such a century time scale. This is typically a vertical mixing time scale h^2/K_v (or a vertical advection time scale) based on a *vertical scale h* appropriate for the main thermocline (about 500 m). This will be supported by further analysis of the dominant heat balance in these regions. On the other hand the adjustment of the deep temperature fields requires far longer times, typically millenia. Although the deep dynamics and kinematics are well established after several centuries, the deep heat balances are not and this is because vertical mixing and vertical advection become rather inefficient to carry heat downward in the abyss while the reverse path to the surface through convection in polar regions remains powerful.

Finally the sensitivity to different initial conditions has been studied by carrying out runs in which the initial stratification is absent: no systematic convergences to other steady states have been observed.

4. Energetics

The next four sections describe in detail the steady solution of the particular run HR1 in Table 1, deferring to the last section the parameter sensitivity study. This three

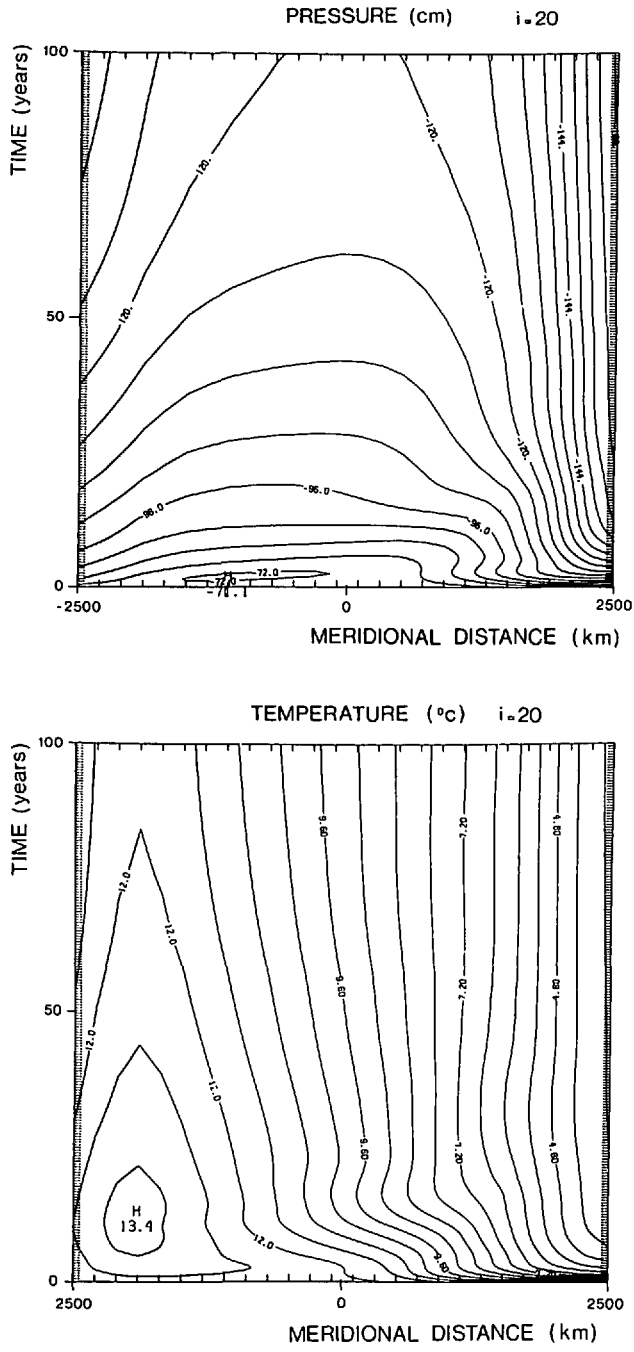

Figure 3. Pressure (cm) and temperature (degree C) in characteristic $y-t$ diagrams at 225 m. The meridional cut occurs in the eastern basin and runs for the first 100 years.

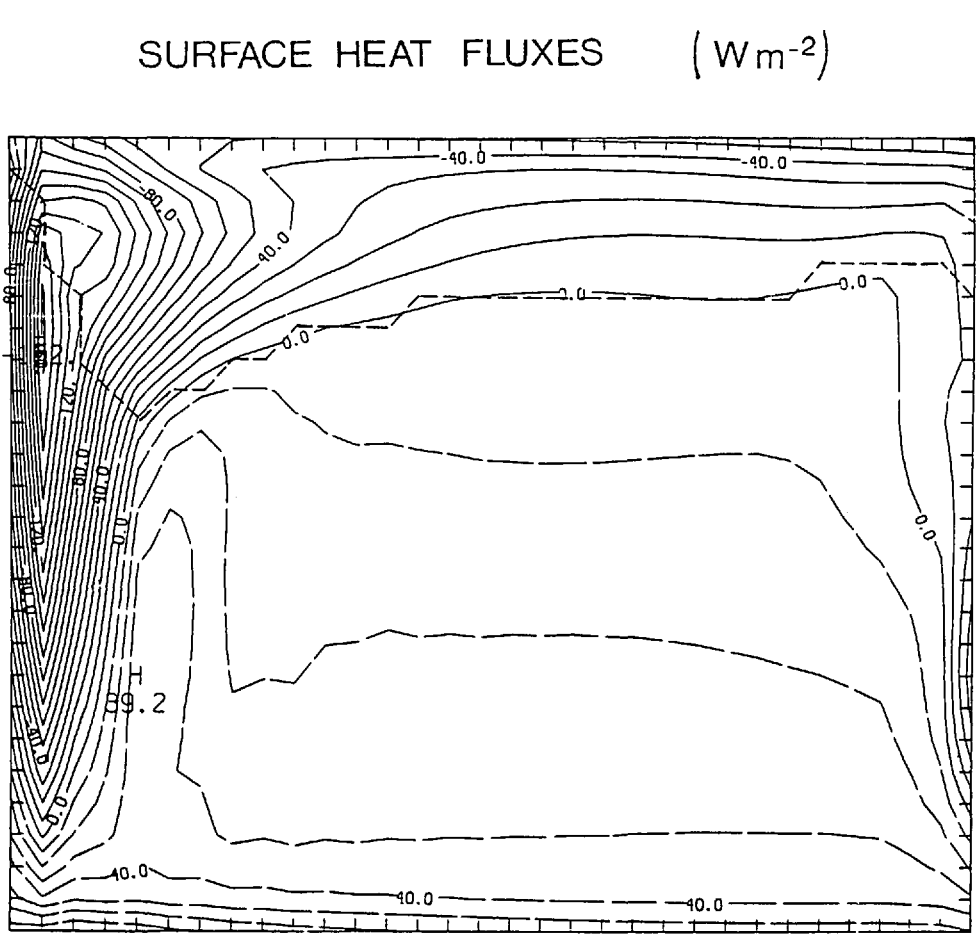

Figure 4. Horizontal map of the surface heat fluxes (watts m^{-2}) in the model. The dashed line is the southernmost boundary of the convection region.

dimensional solution has a complex and rich structure which is robust to parameter changes. The diffusive coefficients used in HR1 (1 $cm^2\ s^{-1}$ and 7 $10^{+6}\ cm^2\ s^{-1}$ in the vertical and horizontal directions respectively) are typical of the large scale ocean but the evidence is of course very limited (Munk, 1966, and Freeland *et al.*, 1975). After integrating the solution for about 800 years, the spatially averaged buoyancy forcing is nearly zero and the residual imbalance corresponds to a global warming of 2.10^{-2}°C per century. The pattern of buoyancy forcing (Fig. 4) is strongly reminiscent of that in the North Atlantic (Bunker, 1976) with an intense heat loss (maximum of 160 W M^{-2}) along the western boundary clearly associated with the warm horizontal advection below and a broader weaker heat gain (20 W m^{-2}) in the interior. Along the eastern boundary a narrow ribbon of negative values occurs and is caused by an intense downwelling along that coast (in nature the opposite usually occurs because of a local response to equatorward winds). The boundary of active convection follows quite

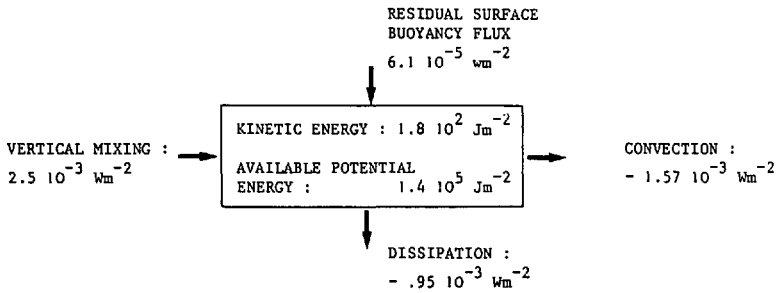

Figure 5. Energy box diagram at steady state of the pivot high resolution run.

closely the line of zero buoyancy flux in the interior but departs from it at both meridional boundaries where advective processes dominate. The steady state energetics are straightforward in such a system: with no net surface fluxes of potential energy, the energy balance occurs through an internal redistribution between the sinks (convection and lateral dissipation) and the source (vertical mixing) (Fig. 5). About 60% of excess potential energy is removed by convection and the rest by lateral friction. Because the potential energy fluxes act in very different parts of the domain (dissipation in the western boundary region, vertical mixing in the southern interior and convection in polar region), the circulation itself is the essential link to allow the system to work: warmed in the interior by vertical mixing from the surface, fluid columns increase their potential energy and are exported to the western boundary region where dissipation occurs. At more northern latitudes excess potential energy removal by convection is possible. Energies are also computed in Figure 5. While the calculation of kinetic energy is straightforward, that of potential energy requires care. The potential energy $\iiint \rho g z \, dv$ is not a useful number because little is actually available for conversion. The far more useful available potential energy (APE) is defined as that portion of potential energy used to level isopycnals adiabatically. It has been roughly estimated here as $\iiint \frac{1}{2} N^2(z) h^2 \, dv$ where $N(z)$ is the horizontally averaged Brunt-Väisälä frequency and h the excursion of an isopycnal away from its resting flat position. This adiabatic leveling is difficult to carry out rigorously in a global domain with surface outcropping of isopycnals: the background stratification varies enormously from stratified southern region to well-mixed northern ones. The operational compromise used here is to calculate separately APE over the southern half and northern half of the domain and then averaging individual values, the nonsatisfactory side effect being that the global background state is not one of no motion. This particular procedure is unlikely to change the results and conclusions implied by Figure 5. APE exceeds kinetic energy by nearly 3 orders of magnitude to reach $1.4\ 10^5$ J m^{-2} reflecting the very large scale of the motions compared to the internal Rossby radius. If this APE value is divided by the observed dissipation of $.95 10^{-3}$ W m^{-2} a time scale of 4.75 years emerges. It represents the time needed for the motion to spin down after impulsive switch-off of the surface buoyancy flux. This time

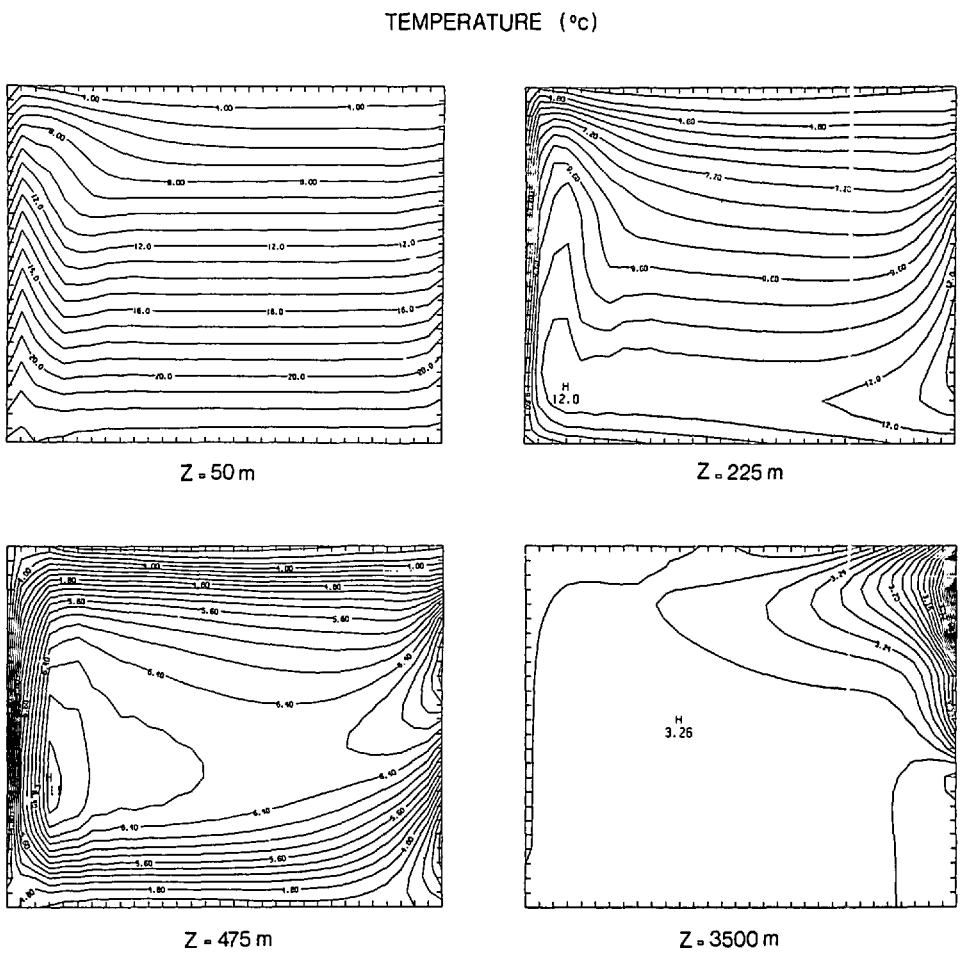

Figure 6. (a) horizontal maps of temperature (°C) above three main thermocline (the first 3 levels) and at the deepest level in the model; (b) horizontal maps of pressure (cm) at the same levels; (c) potential vorticity (units of 10^{-14} cm^{-1} s^{-1}) along a particular isopycnal surface whose topography is given in meters.

scale compares with the shortest time scale found in the problem, namely those associated with the internal Rossby waves or the meridional advection in the western boundary current region. By comparison the stratification of the main thermocline would be mixed away by the small scale diffusive processes on a time scale of 50 to 100 years; i.e., 10 to 20 times more slowly than the large scale motions themselves.

5. The steady state solution

The fields of temperature, pressure and potential vorticity are shown in Figure 6 and they are described carefully to reveal their inner interdependencies. Of course this is a

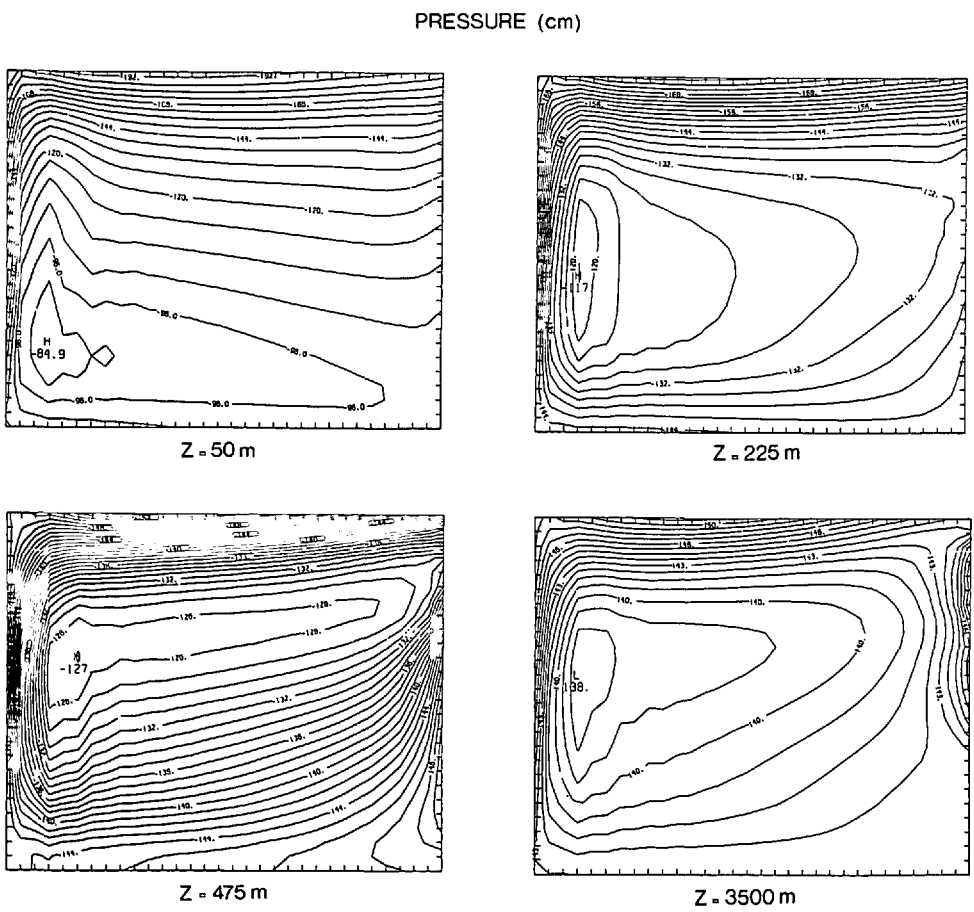

Figure 6. (Continued)

particular solution of a complicated nonlinear system and as such it cannot be used to build more general solutions. The objective is simply to identify and understand features in the various fields.

a. General description. At the surface the temperature field is fairly zonal and reflects the atmospheric temperature. Northward (southward) excursions from the zonal atmospheric distribution in the western boundary region (in the interior) indicate a pattern of horizontal advection intensified in the west, as illustrated on the uppermost pressure map. (The latter is an easy way to diagnose the geostrophic velocity but remember that in this planetary limit the north-south transport between isobars is horizontally divergent.) The surface pressure map shows an intense northward flow at the western boundary which is fed from below rather than by horizontal input from the east. This northward flow overshoots and turns east as a broad current which plunges

POTENTIAL VORTICITY

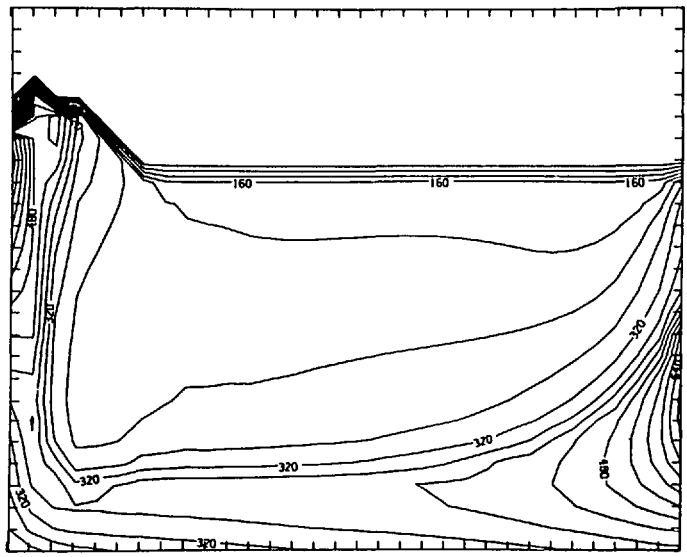

ISOPYCNAL TOPOGRAPHY

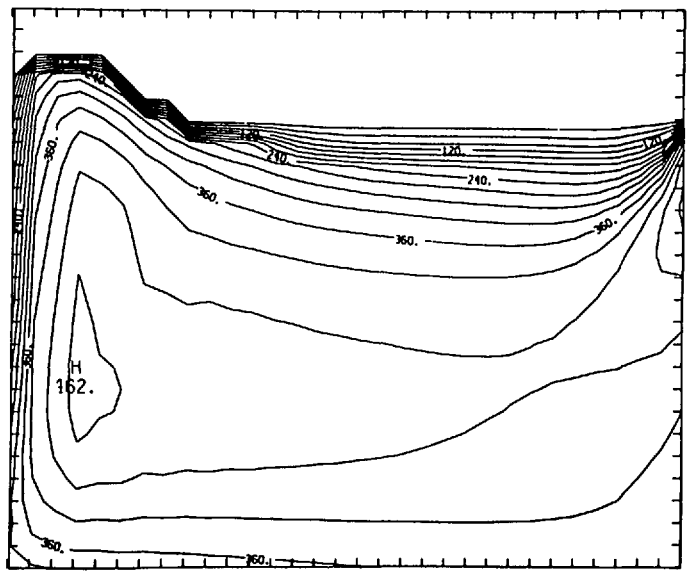

Figure 6. (Continued)

at the eastern boundary. At the next 2 levels down (225 m and 475 m) departures from zonality are stronger: a warm tongue at 225 m originating at the eastern boundary develops in the southern part of the model and reaches the western wall. The pressure map shows increased horizontal recirculation. This is the upper thermocline flow because at level 4 (800 m) the node of the baroclinic mode is reached and apart from eastern boundary phenomena, the circulation is weak. Both warm temperature anomalies and high pressure centers move to the northeast with increasing depths. Note the swift eastward flow found in the convection region and the slower southwestward flow in regions of heat gains, the latter of course reminiscent of a Sverdrup flow in wind driven subtropical gyres. The zonal extension of the warm anomaly is the dominant feature of this solution. At a given level it is induced by downwelling of upper level eastward flows at the eastern boundary. In contrast, the cold anomalies induced by upwelling and air-sea exchange at the western boundary remain trapped there. Both the β effect and advection are important in establishing these patterns. In the northern part the β westward influence and eastward advection oppose each other preventing the warm tongue from developing while in the south both favor westward influence. In a steady state this warm anomaly is made stationary in the interior by upward diapycnal vertical velocities in the main thermocline consistent with the southward motions of the upper layers. Such vertical velocities are indeed observed in the model (Fig. 13). Coming back to the geometry adopted by the gyre, it is seen that the axis of the high pressure lies north of that of the warm pool at the same level. This is just what is needed to transport heat horizontally with warm and cold horizontal advection occurring respectively in the northwest and the central interior. This horizontal heat flux is largest at the surface and decreases at depths as pressure and temperature contours intersect at smaller angles. This pattern of heat transport is also reflected in the vertical veering of current spirals which rotate clockwise with increasing depths in the central interior, the opposite rotation occurring in the northwest. Therefore the interior geometry adopted by the shallow gyres (northward migration with increasing depths) is dictated by the pattern of horizontal advection within the thermal wind constraint (see Section 6(a)). Such northward nesting of gyres has also been explained via potential vorticity homogenization within 2 dimensional recirculating flows (Rhines and Young, 1982). It appears here as a natural response to large scale buoyancy driving.

The potential $q = f\rho_z$ is best described (Fig. 6c) on isopycnal surfaces because q contours on such surfaces give indications of actual flow when nonconservative effects are weak. The chosen isopycnal shows a zonally elongated bowl structure with sharp gradients near the outcrops. Approaching the eastern boundary, the isopycnals turn to the northeast and intense crowding occurs at the point where the outcrop intersects the boundary. This near singularity is made possible by the intense downwelling observed at that boundary. The potential vorticity distribution indicates two outstanding anomalies whose origins can be traced back to the surface.

—A large interior region of low potential vorticity is seen to originate from the convection region. Such direct ventilation of the gyre which occurs without the help of Ekman pumping is carried out by the southwestward flow apparent in Figure 6b. The rather homogeneous distribution reflects more the uniformity of q at injection latitudes than possible horizontal recirculation effects as suggested by Rhines and Young (1982).

—The second region is distinguished by high potential vorticity values with a familiar tongue-like distribution originating at the eastern boundary. Downwelling occurs there to inject the higher potential vorticity found closer to the surface. Again the southwestward return flow of the subtropical gyre advects that anomaly back in the interior with diffusive processes acting along the way. The vertical mixing must be influent to transfer downward high q values from the surface on account of the large stratification found at these southern latitudes. Because of the presence of that tongue, the meridional gradient of q is reversed from what is observed closer to the surface where q decreases monotonically northward as a result of the stratification. This anomaly can be further identified along the western boundary: it is advected northward by the boundary current and rapidly destroyed by convection when finally exposed to the surface.

At depths below the main thermocline, the flow reverses and a large scale cyclonic gyre is found. It intensifies to the west and shows little depth variation, for the horizontal temperature gradients are now small. Intense zonal westward flow fed by an elongated deep water source at the northern boundary is found in the northern part of the basin. It then flows southward as a narrow deep western boundary current and recirculates as a weak northeast current in the interior. This southward boundary current and northward interior circulation are indeed what had been put forward by Stommel and Arons (1960) in their construction of abyssal circulation flows, given specification of interior upwelling and deep water sources. Vertical velocities at level $3_{1/2}$ (600 m) are shown in Figure 13. By nature, vertical velocities tend to show more small scale structure than pressure fields because of repeated horizontal differentiation to obtain them. In spite of this, a large region of positive upward velocities are found in the main thermocline. The pattern is far from uniform but values of interior vertical velocities are maximum at this level and reach 5 10^{-5} cm s^{-1} within the southern region. Along the coasts vertical velocities 10 times larger occur, upwelling being located in the western boundary region and downwelling near the northern boundary. The downwelling intensifies in the northeast corner which appears to be the deep water formation region.

Figure 7 provides two temperature meridional sections in the western and eastern part of the basin respectively. The orientation to the northeast of the warm pool can be traced between the 2 sections. On the whole these temperature sections appear to be realistic analogs of what may be observed in the ocean: stratified waters to the south with isotherms shallowing equatorward with a gradual transition to near vertical slopes

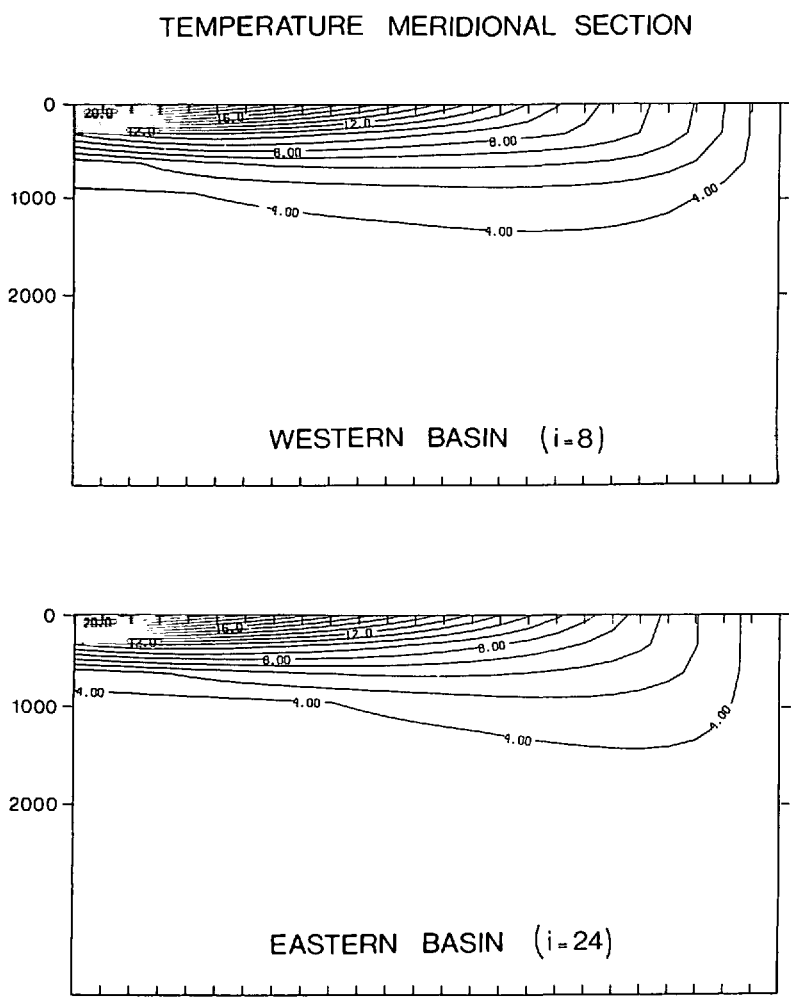

Figure 7. Meridional sections of temperature in the western and eastern basin.

in northern regions. The maximum vertical gradient is present at the surface and decays monotonically below, a situation different from the North Atlantic where a large gradient can be observed around 850 m (shallower in the Pacific). Clearly some processes are missing to reproduce that important feature. Layer between isotherms thicken to the north, implying that stratification is able to compensate and even override the β effect creating the plateaus in the potential vorticity $f\rho_z$ shown earlier. Significant southwestward interior flow above 600 m occurs in these regions of reduced potential vorticity gradient. By contrast, in polar regions the geometry of the nearly vertical isopycnals imposed by convection inhibits meridional flows because the

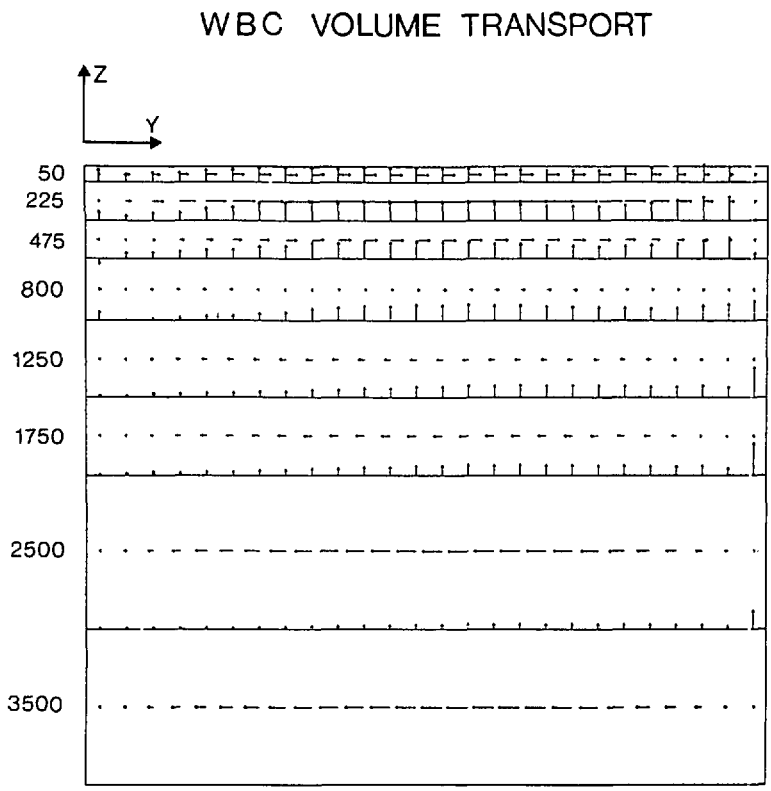

Figure 8. Vertical structure of the volume transport of the western boundary current: maximum horizontal arrows represent 10.5 10^{+6} m^3 s^{-1} and maximum vertical arrows 0.55 10^6 m^3 s^{-1}.

fractional change in thickness cannot be accommodated by similar fractional changes in planetary vorticity: the flow adjusts by speeding up zonally.

b. Boundary currents. The two gyres, anticyclonic at the surface and cyclonic at depth, are strongly asymmetric in the zonal direction. As in early homogeneous models, a boundary layer current occurs at the western boundary, the novelty here being the nontrivial vertical structure. The net transport is zero and the node appears to be shallow (around 600 m). Figure 8 shows the vertical structure of the horizontal and vertical transport averaged over the boundary width which scales as in Munk's problem. The maximum transport in each branch (northward or southward) is about 20 10^6 m^3 s^{-1}, maximum at a latitude of 40°. The generalized upwelling that occurs along the western boundary is the consequence of heat convergence from both horizontal advection which transports warm subtropical water to the north and horizontal diffusion acting across the sloping isotherms. Cooling through the upwelling is needed to achieve steady state balance. Veronis (1975) has pointed out that the

upwelling at the boundary in one of Holland's (1971) simulations was entirely induced by the large diffusion coefficient which also forced downwelling in the interior of the fluid. In the present simulation the horizontal advection of heat is important in the boundary layer and helps horizontal diffusion to equilibrate vertical advection above the main thermocline. That is, the boundary upwelling appears to be a genuine feature of the circulation, the diffusion processes providing only the necessary adjustment to boundary conditions. Furthermore this upwelling at the western boundary is favored by the present buoyancy driving: the small amplitude solution (Section 9) consists of upper (lower) eastward (westward) flows closing their circuits via upwelling (downwelling) at western (eastern) walls. In the more realistic finite amplitude case upwelling is intensified compared to the downwelling through horizontal advection and diffusion processes enhanced at the western boundary. At no times is it such as to induce downwelling in the interior as in the case discussed by Veronis.

In each depth range a certain amount of horizontally transported water comes from vertical mass exchange: in the three deep layers the southward WBC is fed by a large westward flow near the northern boundary but is subject to vertical divergence as well, for the transport weakens and joins the interior as a much reduced eastward flow. The opposite occurs in the two uppermost layers in which the equivalent Gulf Stream, initially weak at the south, gathers its strength by two processes: new fluid enters the boundary from the side as in homogeneous models while at the same time vertical convergence also increases the transport. As the WBC reaches the northern boundary, fluid exits to the east as an intense zonal current. Within the main stream, the WBC is flowing down the pressure gradient a possibility offered by momentum dissipation at the boundary. As possibly more is known about the general circulation in WBC than anywhere else, there are 3 features of this simple simulation that are not easily reconciled with observations: the first deals with the vertical structure of the WBC: observations show that the Gulf Stream extends to the bottom (Richardson, 1985) and the DWBC situated inshore of the Gulf Stream is found between 2000 and 3000 m (Hogg, 1983). By contrast the model baroclinic Gulf Stream changes its direction at shallower levels. Second the model upper layer WBC transport is of course too weak and third the Gulf Stream does in fact leave the coast near the latitude of the Grand Banks. These two latter aspects of course come from the missing wind forcing whose effects in combination with the buoyancy forcing will be reported elsewhere. The vertical structure problem may have additional causes.

As can be seen on the deepest pressure maps in Figure 6 a northward eastern boundary current is also present. It reappears at 800 m as a southward eastern boundary current. This boundary current communicates little with the interior. The vertical velocities along the eastern boundary around 1500 m close the flow as a *vertical* loop circulating fluid in the meridional yz plane in a clockwise sense looking eastward. The presence of the boundaries appear to induce significant divergent flow in

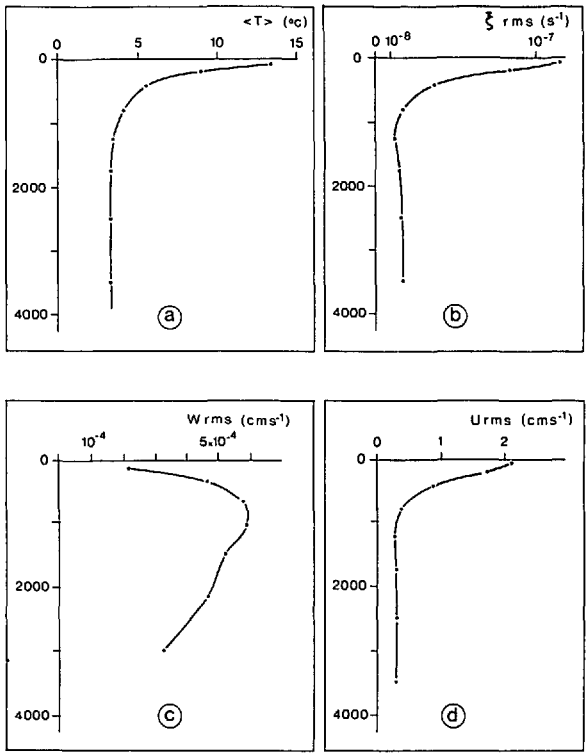

Figure 9. Vertical structure of horizontally averaged quantities in the model: (a) mean temperature (b) rms relative vorticity (c) rms vertical velocity, (d) rms horizontal velocity.

these experiments that scaling would have excluded on the assumption of small Rossby number flows.

*c. Statistics.*This general description is completed by presenting some statistics in Figure 9. Spatial mean and variance have been computed for several quantities: temperature, horizontal and vertical velocities, vorticity and horizontal divergence. Gross vertical structure of these quantities shows the vertical intensification of the circulation near the surface and involve a mean thermocline *e*-folding depth of about 550 m. The vertical rms velocities are maximum at mid-depth in the center of the main thermocline. Finally rms vorticity exceeds horizontal divergence by typically an order of magnitude: hence, although intense vertical velocities occur near the boundaries, horizonally recirculating flow dominates the kinematics. It is otherwise for the heat transport as demonstrated in Section 7.

Through this general description, it is hoped to have demonstrated that these solutions do not appear to be so unlike the ocean as to prevent more detailed analysis. This is needed because an important question has not been answered: why after all is the flow anticyclonic (cyclonic) above (below) the main thermocline?

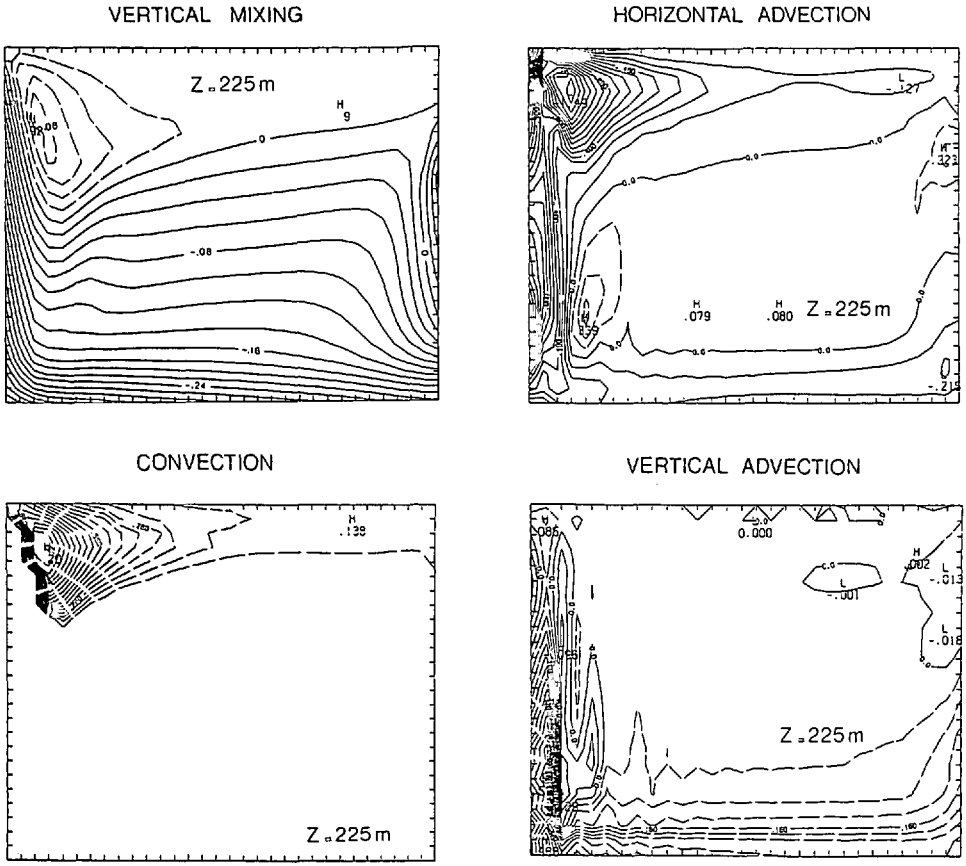

Figure 10. Horizontal maps of various terms of the density equation given adimensionally at 225 m. In regions of heat losses, a balance between warm horizontal advection and convection is found while in region of heat gain, cold horizontal advection and upwelling balance vertical mixing. Positive numbers (negative) imply positive (negative) density tendencies.

6. Heat and vorticity balance

The key to answer such a question is the distribution of vertical velocity in the model interior because the stretching term in the vorticity equation is the decisive contributor. More fundamentally one may hope to identify which terms in the full density (or heat) equation equilibrate the vertical velocity. The main result of this section is that the natures of the heat and vorticity equilibria are regionally dependent.

a. The heat balances. Each term of the density equation (10) has been computed at each level of the model in order to determine the important balances in the main thermocline. Attention is first restricted to regions of heat loss to the atmosphere: Figure 10 shows the important terms at level 2 (225 m). Starting from the top, the

buoyancy forcing is balanced by warm advection in the WBC region and by convection along the northern boundary. At level 2 and 3 (225 m–475 m) warm advection in the boundary current equilibrates with cold upwelling at the boundary and horizontal diffusion. At level 2 along the northern boundary, a region 1500 km wide, heat transported initially by the WBC is flushed out by convection. Vertical advection is very small compared to both terms because the water is very weakly stratified: its sign is associated with that of a cold upwelling. Going deeper (level 3) the convection region shrinks to the north and the associated above balance as well. To the south of the convection region, a stronger stratification prevails and warm advection and vertical mixing are balanced by increased cold upwelling from below.

The situation is rather different in the much broader regions of heat gain, excluding the WBC, the northern regions discussed above and the narrow coastal areas along the eastern boundary. At upper levels cold horizontal advection from the north and upwelling balance the warming influence of the atmosphere above (vertical mixing). These regions are strongly stratified and have rather weak horizontal currents, both of these factors contriving to give at greater depths *a dominant balance between warming by vertical mixing and cold upwelling* (see Fig. 11). Both fields correlate visually, increasing to the east and decreasing to the north. The underlying positive vertical velocities are maximum at the base of the main thermocline; i.e., between 600 and 800 m (Fig. 13). This particular balance underlies most early thermocline theories and it is shown here to hold in regions of heat gain.

At abyssal depths, the stratification is again weak and vertical mixing becomes inoperative to bring heat downward. The equilibria are complicated and not totally steady. Schematically horizontal diffusion and advection equilibrate the heat loss by convection which now occurs in a very small region at the northern boundary. Downward heat transport relies on vertical downwelling in the northeast corner and in the western boundary region. In the rest of the domain both horizontal diffusion, horizontal and vertical advection assume various balances. Both the eastern and western boundary regions are warmed by horizontal advection. Although the heat transports at abyssal depths are important for global heat equilibria in the system, they do not play a great role in the dynamics which are dominated by thermodynamic processes occurring in the main thermocline.

b. The vorticity balances. The vorticity tendencies in different regions must obey Eq. (3). The vertical velocities reaching a maximum at the base of the main thermocline (Fig. 12) imply that vortex stretching is best illustrated in the upper thermocline. The large scale pumping in the interior is bound to produce a large scale negative vorticity tendency and this is indeed what the upper layer anticyclonic flow shows. The reverse occurs below since the vortex stretching now becomes positive. On inviscid grounds southward interior velocity should occur at shallow depths and northward flow below if the beta term equilibrates stretching, the viscous stresses allowing intense return flow

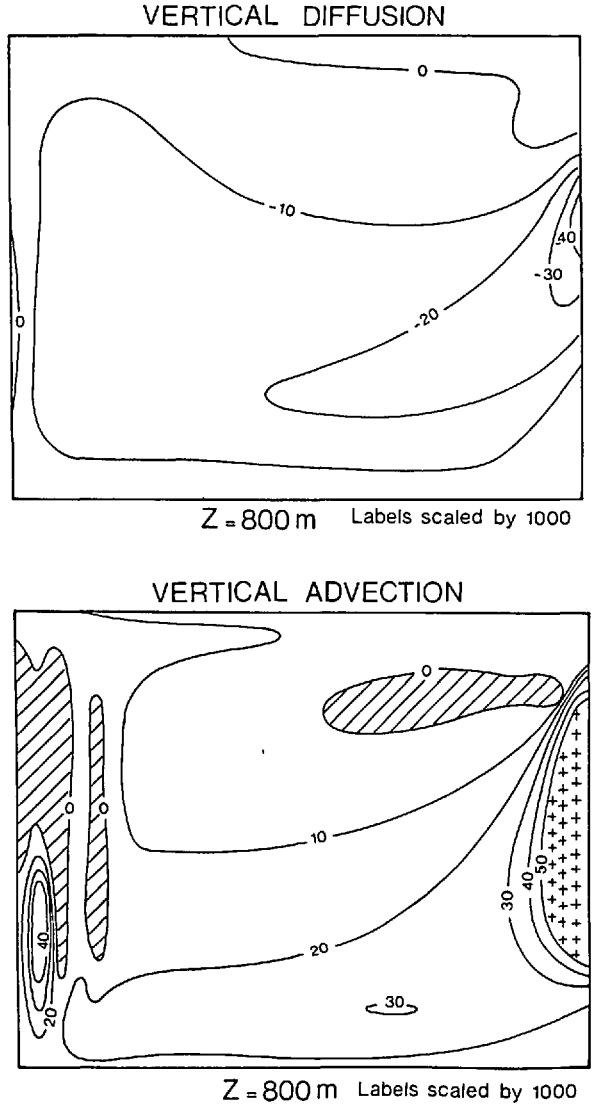

Figure 11. Horizontal maps of the dominant contributors of the density equation at 800 m. In the southern part of the model a balance between upwelling and vertical mixing develops (negative values in the vertical advection are dashed and extrema have been indicated by +). The sign convention is as in Figure 10.

at the western boundary. On the whole this is what happens in the model (see the pressure field in Fig. 6): to test quantitatively the "$\beta v = f w_z$" balance both terms have been computed in the model subtracted from each other and divided by the sum of their absolute values. The result obtained in percentage values is shown at level 2 (225 m) and 7 (2500 m) in Figure 13. The inviscid balance is obtained approximatively in the

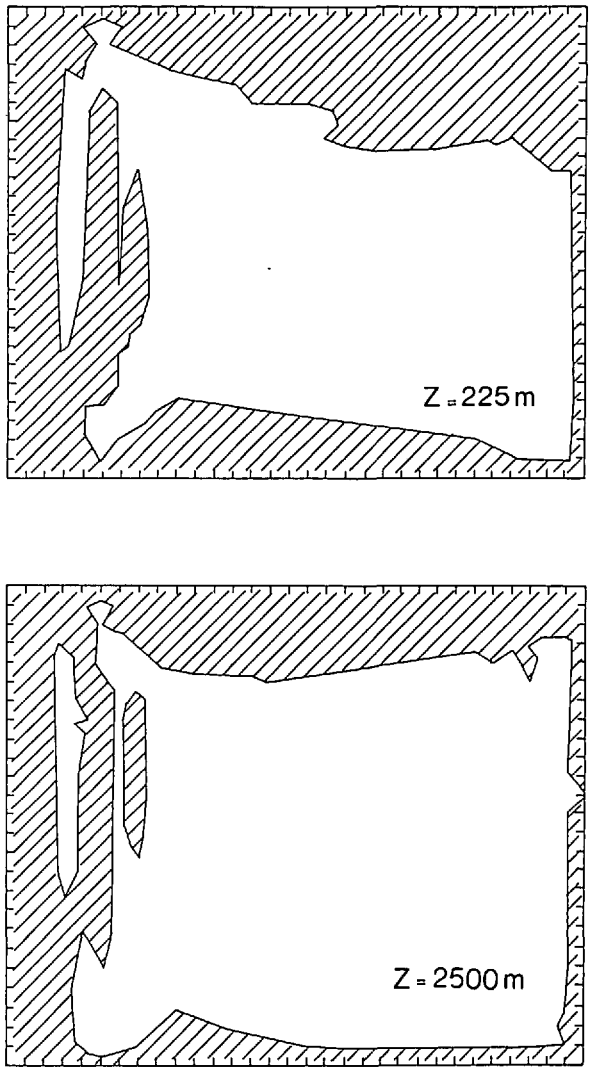

Figure 12. Planetary vorticity balance testing at two levels: the area where that balance is invalid by more than 50% is shaded. The western boundary current region and the convection area stand out as regions in which friction is important.

southern interior of the gyres both at shallow and abyssal depths: it is particularly instructive to note that the approximate inviscid balance checks very close to the eastern boundary but not at the eastern boundary. Adjacent to the boundary, mass is redistributed vertically to satisfy the boundary conditions at the wall, producing very large stretching terms which cannot be equilibrated by planetary vorticity alone. Lateral vorticity diffusion takes hold in that boundary layer whose width is not resolved in the model. In their study of the ventilated thermocline Luyten *et al.* (1983)

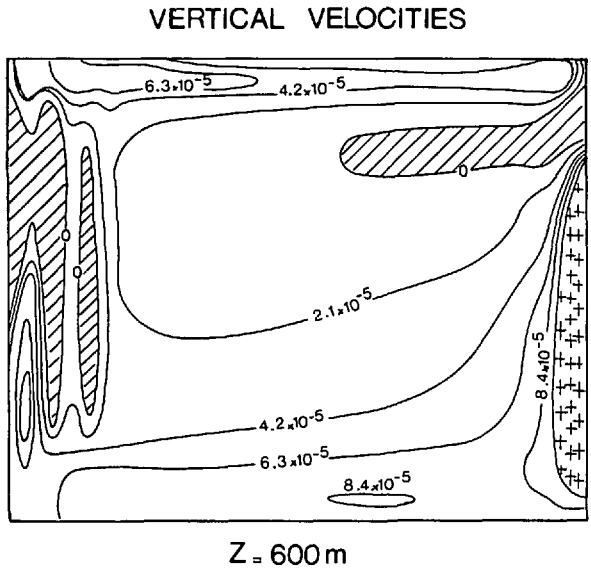

Figure 13. Horizontal map of vertical velocity at 600 m. Intense values at the grid point adjacent to the boundary have been marked with + and negative values are dashed. Interior vertical velocity is maximum at this level.

present wind-driven solutions in a layered model ocean with specified positions of the isopycnal outcrops. Some aspects of the buoyancy forcing at the surface are therefore implicitly taken into account in their choice of physics. Total adherence to the planetary vorticity equation along with the condition of no normal flow at an eastern wall gives the very special character of their calculated flows with isopycnal thicknesses vanishing at the eastern wall. The present solutions suggest instead to integrate the planetary vorticity equation in the westward sense starting outside a thin buffer layer. The full 3D circulation being coupled by vertical mass redistribution in that buffer layer, it is difficult to imagine how to find *a priori* the velocity boundary conditions to apply west of that layer.

That the inviscid vorticity balance should not be good near the western boundary is no surprise because vorticity dissipation helps to restore the absolute vorticity of a fluid parcel to the appropriate planetary value at the exit latitude. The surprise comes in fact from the northern boundary region, an area of heat losses as was shown earlier. Both at shallow and deep levels, the inviscid vorticity balance is 100% wrong. At shallow levels the geometry of the isopycnal outcrops is entirely dictated by convection and the meridional slope of the isopycnals becomes very large. Furthermore at the boundary between stable and unstable regions the potential vorticity is discontinuous. There is just no way that the beta terms can be important in such a rapidly varying isopycnal geometry: the fluid adjusts by moving zonally and the negative vortex stretching still present at upper levels is now equilibrated by lateral diffusion of vorticity. At abyssal

levels, the westward moving fluid suffers similar positive stretching again equilibrated by vorticity diffusion. That these zonal flows are horizontally divergent is quite a novel feature. This divergence depends on quite a subtle imbalance between convection and horizontal advection of heat in the upper layers. As the flow is weakly stratified a small imbalance can lead to rather large vertical velocity. Suppose that at a given level convection and warm advection balance. Since the convection zone shrinks northward with depth, it appears that the only way to balance the warm advection at greater depths is by cold upwelling hence the negative stretching above which is then caused by the unequal vertical penetration of convection and warm advection (allowed by the component of the flow acting across the thermal front).

Finally we must emphasize that the test of the vorticity Eq. (3) carried out here is different from the test of the conservation of potential vorticity f/h between 2 isopycnals of thickness h; i.e., the vanishing of the right-hand side of Eq. (11). This implies a partition of the total vertical velocity between components acting along and across isopycnals. The dominant heat balance in regions of heat gains exposed previously shows that the cross-isopycnals component is important and represents a local driving for the meridional flows. A reconstruction of potential vorticity balances along isopycnals would be desirable to quantify in more general situations how subsurface flows are driven locally or remotely at outcrop windows.

c. Stommel-Arons dynamics. It now must be apparent that these steady state solutions have some qualitative similarities with the construction of abyssal circulation patterns by Stommel-Arons (SA in the following). The simplified heat balance dominated by vertical transport processes and the northward interior abyssal flow which occur in heat gain regions of the model are indeed familiar features of their abyssal circulation. The purpose of this paragraph is to show the overall agreement between the model results and SA predictions, the transport of the deep western boundary current (DWBC) being chosen as the major index of the SA schemes of circulation. The model interior vertical velocity maximum at a level z_c of 600 m (Fig. 14), is chosen to predict the strength of the DWBC following the SA prescriptions. The DWBC transport T_w occurs as a mass balance residual between water leaking above to the main thermocline and horizontal northward advection induced by the vortex stretching terms. In the interior, we have:

$$\beta \int_{-H}^{z_c} v \, dz = fw(z_c). \tag{12}$$

Mass conservation for that part of the basin limited to the north by a control latitude y implies that the DWBC transport $T_w(y)$ obeys:

$$T_w(y) + \int_{X_w}^{X_e} \int_{y_s}^{y} w(z_c) \, dxdy + \int_{X_{bc}}^{X_e} \int_{-H}^{z_c} v \, dz = 0$$

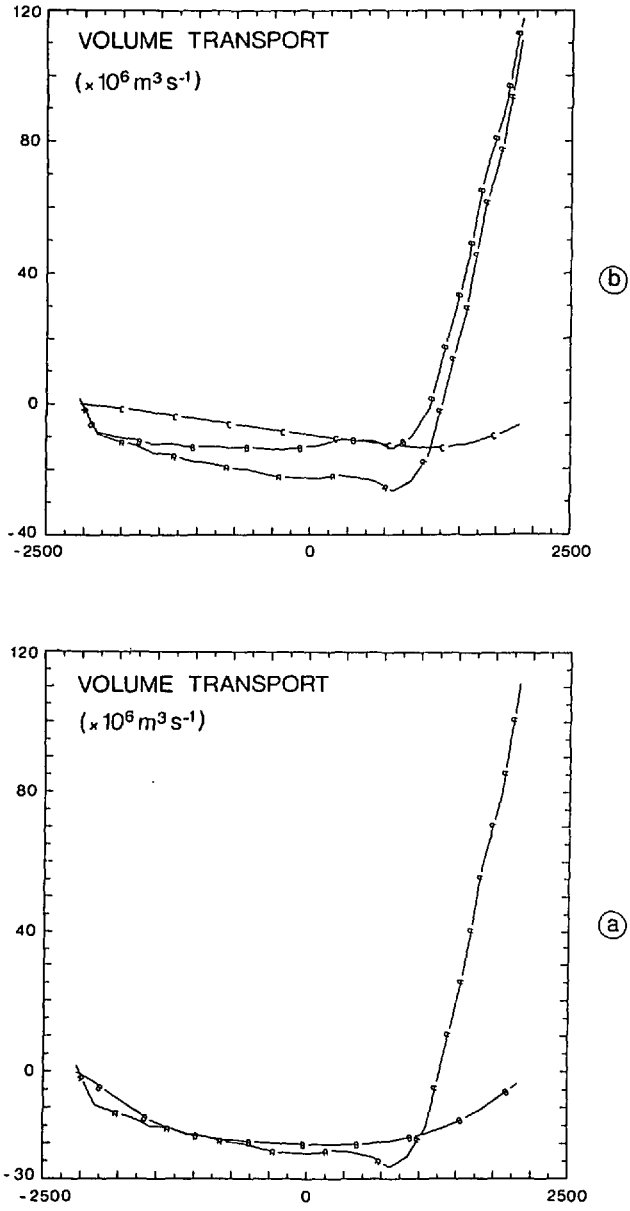

Figure 14. (a) Volume transport of the deep western boundary current in the HR run. Curve A is the Stommel-Arons boundary current transport and curve B is the observed model transport. (b) Different contributors to Stommel-Arons' transport. Curve B represents the integrated interior upwelling, curve C the interior horizontal leakage to the north provided by the β effect and curve A the sum of the two.

where X_w and X_e are western and eastern boundary coordinates and y_s the southern boundary. X_{bc} is the offshore extension of the DWBC so that $T_w(y)$ is defined as:

$$T_w(y) = \int_{X_w}^{X_{bc}} \int_{-H}^{z_c} v \, dz. \tag{13}$$

By using the vorticity equation (11), one obtains

$$T_w(y) = -\int_{X_w}^{X_e} \int_{y_s}^{y} w(z_c) \, dxdy - f/\beta \int_{X_{bc}}^{X_e} w(z_c) \, dx. \tag{14}$$

In this final expression, T_w can be computed from the southern boundary to a latitude just short of the position of the deep water source confined to the northern boundary (Fig. 14). If it were not for the last term in (14) the transport would increase regularly toward the source, being equal to the source strength close to the source. The last term is a horizontal recirculation term which can increase the transport beyond the value of the deep water source. The numerical model providing the vertical velocity, the SA transport $T_w(y)$ was computed as in (14) and compared with the observed model transport computed as in (13) where the meridional velocities are observed model velocities. The results (Fig. 14) show that the transports agree well over the southern 2/3 of the basin and are of the order of 20 Sv at the central latitude. In the northern region however the model transport decreases slowly to zero at the north boundary while the SA estimate departs from it markedly, with huge northward transport. This is again confirmation of earlier results that the simple vorticity balance (12) does not work in heat loss regions. Both contributors in the RHS of (14) are shown in Figure 14. The β recirculation term dominates in the south while the first term increases regularly northward. It is the β recirculation term which induces the SA transport estimates to depart from the observed transport in northern regions. Positive vortex stretching keeps requiring northward interior velocities while model flows in that region are mostly zonal. Looking at the recirculation itself, the maximum southward transport of 20 Sv occurring aroung 40° latitude is larger than the deep water source at the northern boundary (13.5 Sv). The ratio of the two can be defined as a recirculation index which is therefore about 1.48. Scaling of (14) would suggest a recirculation index of the order of the Earth radius divided by the meridional extension of the basin or about 1.3 in the present case. For comparison, McCartney and Talley (1982) estimate a total of 11 Sv of newly formed deep water in the North Atlantic, 8.5 Sv of Labrador Sea origin and 2.5 Sv from the Norwegian Sea. Estimates of the deep western boundary current are variable: Richardson (1977) estimated it at about 24 Sv off Cape Hatteras. Using far more intensive direct current measurement, Hogg (1983) estimates about 10 Sv of southward flow of thermohaline origin above the 4000 m isobath whereas further north DWBC increase to about 30 Sv due to the presence of horizontal gyrelets possibly driven by eddy stresses. Therefore while model and observations appear to be in the same range of values, the degree of recirculation in the ocean due to the existence of an interior upwelling is not well determined.

To summarize what probably is the main point of this study, it has been shown that in regions of net heat gain (the subtropical region) the steady state model solution follows qualitatively the heat and vorticity balance of early thermocline and abyssal circulation theory. Maximum upward interior velocities cause vertical advection to balance downward heat transport by vertical mixing, and induce interior planetary advection to the south (north) above (below) the main thermocline. The transport of the deep western boundary current is accurately reproduced by the simplified interior vorticity balance between vortex stretching and planetary advection. Along with the thermodynamic origin of the interior vortex stretching term, this may be seen as a confirmation of SA original ideas. In subpolar regions on the other hand in which convection is strongly active, the above ideas do not appear relevant: although horizontal divergence similar to what is observed further south is still present, horizontal currents respond by moving zonally. The heat balance is a subtle one between vertical advection, convection and horizontal advection in which the low vertical stratification acts as an amplifier for vertical velocities and stretching. Lateral diffusion of vorticity takes hold to balance vortex stretching, invalidating Stommel-Arons' ideas in these regions.

7. The zonally averaged circulation and heat transport

Because the net heat source vanishes at the surface of the model ocean, heat must be transported northward because of north-south differential heating. The objective here is to assess how the baroclinic circulation manages to transport heat: this is not a trivial matter because flows in thermal wind balance are severly constrained to do so on a rotating earth. At each latitude the meridional heat flux, zonally and vertically averaged, must export the heat input south of that latitude (Fig. 15). This heat flux may occur by advection and (or) lateral diffusion, the sum of the two balancing the heat source in a steady state. Meridional advective fluxes dominate over diffusive ones except at subpolar latitudes. They reach a maximum density of $1.3\ 10^4\ \mathrm{Wm}^{-2}$ in the center of the basin, a climatological value somewhat on the low side. It was shown earlier that vorticity diffusion was large in the convection region and the same is true of the diffusive heat transports. The vertical distribution of the advective fluxes is shown in Figure 16. At southern latitudes, they are dominated by the *mixed layer transports*. This is because the isotherms forced by the atmosphere are mostly zonal. Below the mixed layer the fluxes are small and sometimes oriented southward: it is at these levels that the thermal wind constraint most effectively prevents large heat transport. Although the net transport is small, recall that the shallow geometry of the gyres (northward migration with depth of the gyres) was a consequence of horizontal heat advection. Within and below the main thermocline the northward fluxes have an interesting tilt, the positive contribution coming from more northern latitudes with increasing depths. Deep sinking occurs in a stratified region in the northeast corner producing a warm anomaly there while convection produces cold anomalies west of the

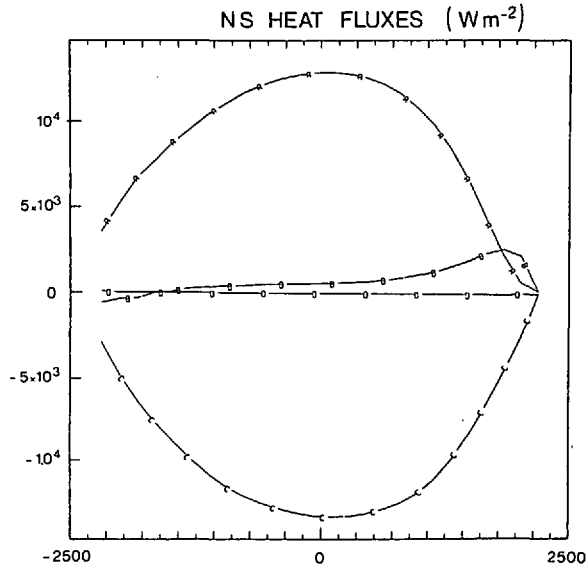

Figure 15. Horizontal heat fluxes across a zonal section as a function of meridional distance given in Watts m^{-2}. Curve A is the advective contribution, curve B the diffusive one, while curve C represent the integrated heat input at the top south of the control latitude. Curve D is the sum of the three which must be zero in the steady state. The value of the maximum advective heat flux at the center of the model is about 0.3 10^{15} watts after multiplication by the area of the vertical section (2.4 10^{10} m^2).

region of active sinking. The small meridional component of the circulation forced by deep water formation at the north boundary and acting on these anomalies is responsible for these positive heat fluxes.

Another way to look at these advective fluxes is to expand the velocity into its rotational and divergent components and compute the heat flux due to each component. This is perfectly defensible because the mass flux of each vanishes across a vertical zonal section. The result (Fig. 17) is instructive: over most of the domain the meridional heat transport is dominated by the divergent velocity component. In particular the rotational part of the fluxes is even transporting heat toward the warm source in the southern part of the basin! Although the divergent velocities are an order of magnitude smaller than rotational velocities, they dominate the heat transport on account of their large horizontal scale and of the large temperature difference between the northward moving branch at the surface and the southward return flow at depths. Strongly recirculating horizontal flows operate against much smaller horizontal temperature gradient leading to weak heat transport. Roemich (1980) came to the same conclusion when estimating Atlantic heat transport at 24 and 36N. A quantity which shows particularly well the circulation responsible for a large part of these heat transports is the zonally averaged circulation in the y-z plane (Fig. 18). After such zonal averaging, the rotational part of the circulation disappears, the net result being a

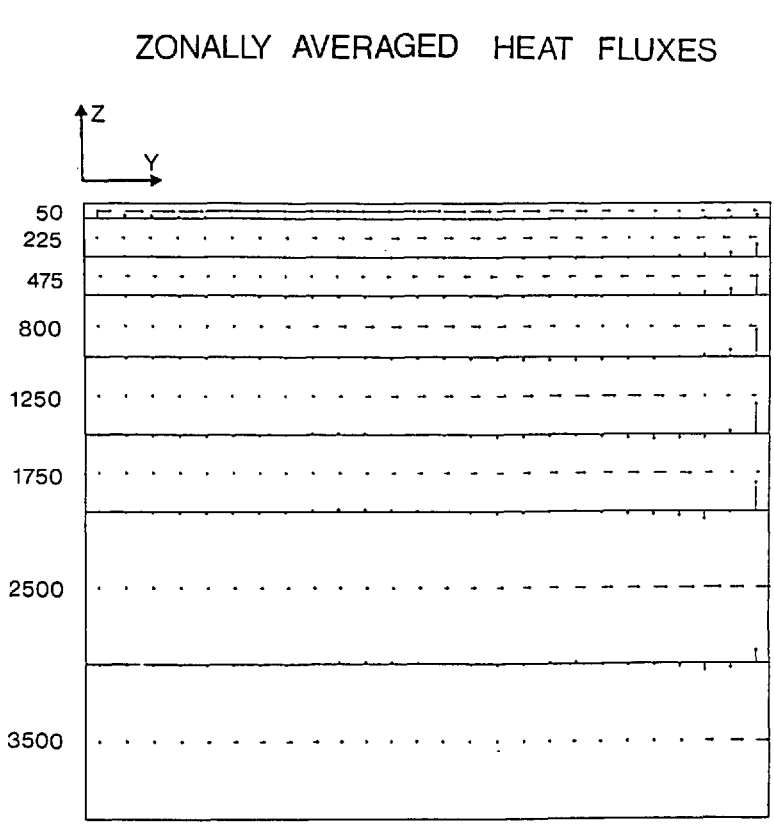

Figure 16. Meridional section showing how the zonally averaged advective fluxes vary with depth. Note the large contribution in the mixed layer, the small sometimes negative contribution at level 2 and 3 and the contribution of the northern region below the thermocline.

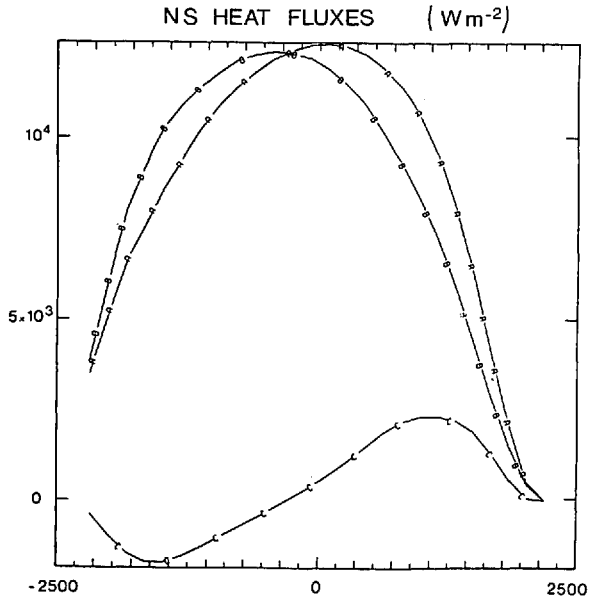

Figure 17. Meridional heat fluxes contributed by the divergent (B) and rotational (C) part of the horizontal velocity field. Curve A is the sum of the two. The heat transport is mostly carried out by the slow, large scale divergent flow.

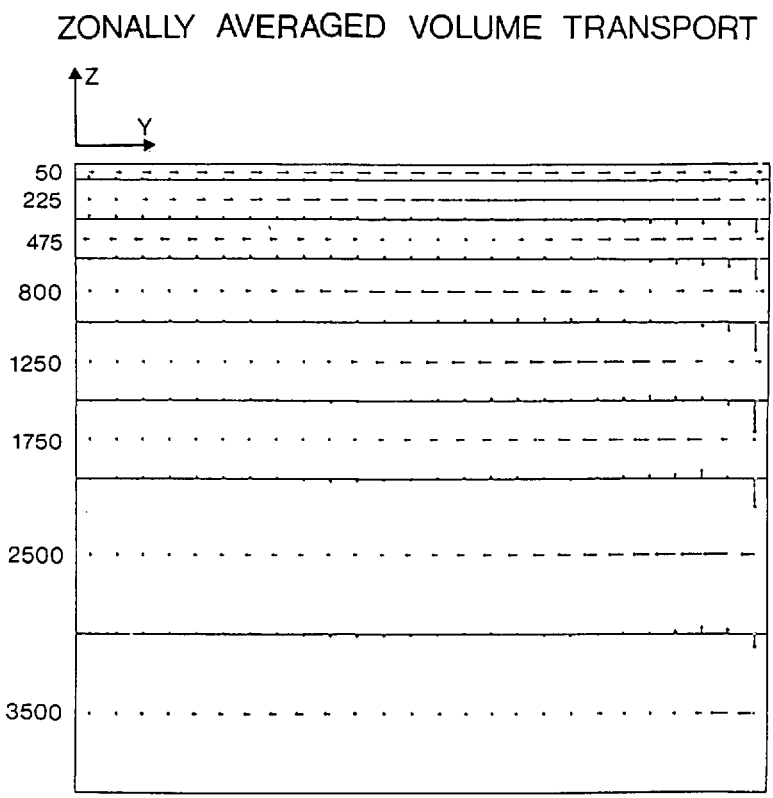

Figure 18. The zonally averaged volume transport in the $y-z$ plane. Maximum horizontal arrows represents 7.4 10^6 m^3 s^{-1} and maximum vertical ones 10.3 10^6 m^3 s^{-1}.

Hadley cell playing the role of a heat exchanger between the warm and cold source. The northward branch is shallow being limited to the first 3 levels and transports about 9.5 Sv in the center of the basin. The return flow below the main thermocline is much broader. Sinking at the northern boundary occurs at a rate of about 13.5 Sv which is returned as a weak upwelling distributed over the whole range of latitudes and particularly evident around 500 m. One must contrast the sense of this circulation with that of the interior Stommel-Arons branches of the circulation. Coming back to the vorticity equation (3), horizontal area averaging $(-xy)$ shows that:

$$\beta \bar{V}^{xy} = A \overline{\nabla^2 \xi}^{xy}.$$

The net meridional circulation which occurs at a given level is driven by lateral diffusion of vorticity, the vortex stretching constraint vanishing upon spatial integration. Because the term on the RHS is dominated by vorticity diffusion within the western boundary current, it is approximately $-A\bar{V}^{y}_{xx}$ at the western end. This quantity is positive (negative) above and below the main thermocline agreeing in sign

with that of the zonally averaged circulation. The zonally averaged divergent circulation is therefore driven by ageostrophic western boundary stresses which are dominated by rotational velocities. In other words although the rotational part of the circulation does not play an important role in the heat transport it helps to drive a net divergent flow important for the heat transport! This shows in particular the subtle influence of the frictional processes in the thermodynamics and the importance of including them in an energetically correct way. These frictional processes help to break the powerful angular momentum constraint on a rotating earth enabling net meridional flow itself important for the heat transport. Although it has been said earlier that eddy diffusion is not important in the heat transport, eddies are nevertheless implicitly present in the boundary current to provide the right vorticity diffusion acting as forcing for the zonally averaged flow.

8. *f*-plane circulations

This is a brief parenthesis in this paper for such a neglect of the earth curvature is not geophysically relevant at planetary scales. It is meant as a curiosity, and curiosity indeed it may arouse as the pressure fields from shallow and deep level in an f plane run (otherwise similar to the pivot run LR in Table 1) revealed in Figure 19. Anticyclonic flow (cyclonic) is found at shallow (deep) levels, a similarity with the β plane case. This is again caused by the large scale upward velocities found at the base of the main thermocline. Such squashing in the upper layers is entirely balanced by lateral vorticity diffusion producing a negative vorticity hence a pressure high. Figure 19 also shows a familiar feature, the northward migration with depth of the gyres in the upper layers, a fact already attributed to the necessities of horizontal heat transport in a fluid in approximative thermal wind balance. The absence of a zonally elongated tongue in density maps shows that the earlier attribution of these tongues to the β effect is correct. However more surprising is the apparent zonal asymmetry revealed in the upper layer flows. With no β effect and on the basis of previous experience with homogeneous model, no western intensification should be expected. This appears not to be true of the surface flow which appear to be western intensified albeit to a lesser degree than with β operating. The energetics and thermodynamics of this run are similar to the β plane runs and the remaining objective here is restricted to pin down the origin of the zonal asymmetry. The first question that comes to mind is whether this is at all possible? Looking at the inviscid set (1), it is readily apparent that the equations are invariant under the transformation $x \rightarrow -x$, $v \rightarrow -v$ and $w \rightarrow -w$. With friction and diffusion added this invariance is lost. This has nothing to do with the variations of f and holds also for the primitive equations. This implies that there are no theoretical reasons to expect zonal symmetry in the present PG f plane frictional, diffusive flows. This must be contrasted with the *linear* quasigeostrophic set for the frictional f plane flows have in that case a built-in zonal symmetry which is lost as soon as f varies. This is of course the case considered by Stommel (1948) in his original

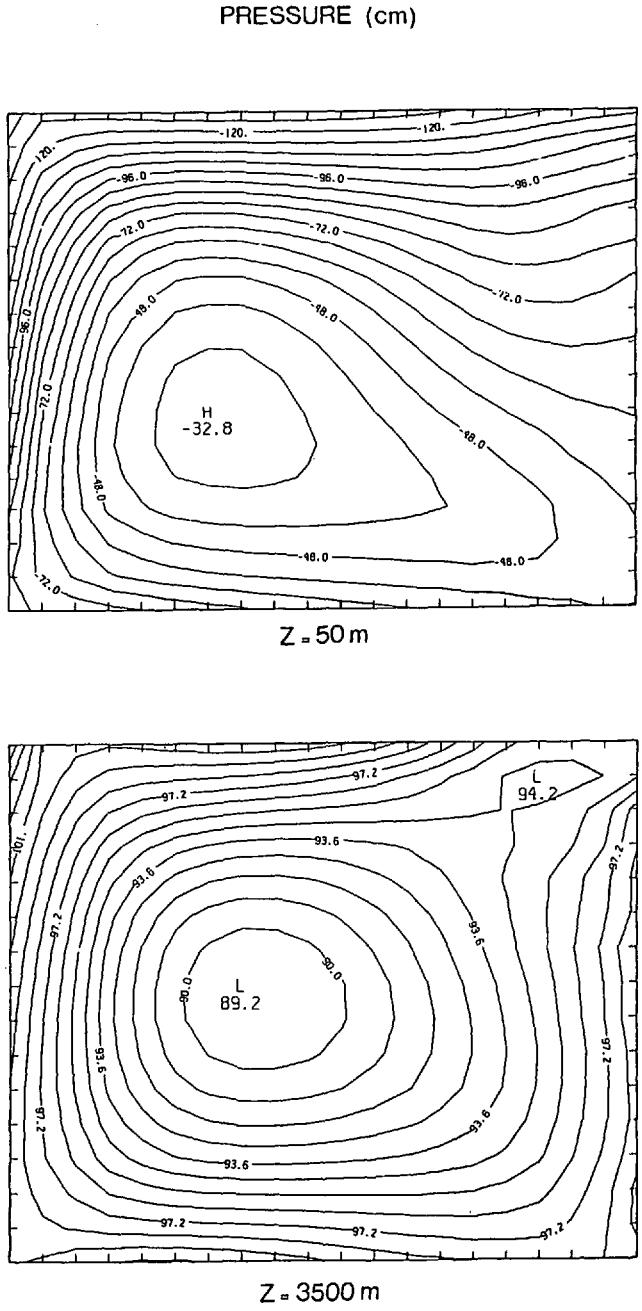

Figure 19. Horizontal maps of pressure (cm) in the f plane runs. This run (low resolution) was carried out with the same forcing as the pivot β plane run described in the text (K_v = 1 cm^2 s^{-1}, K_H = 10^7 cm^2 s^{-1}). (a) the mixed layer, (b) the abyssal layer. Note the small western intensification in the mixed layer.

explanation of the Gulf Stream. The upper layer f plane western intensification observed above may be looked at as follows: a fluid parcel transported in the upper layers of the anticyclonic gyre, the sign of which is given by the mid-thermocline heat balance, suffers heat loss by convection in the north and warming by vertical mixing in the south. The former is an efficient process compared to the other and therefore needs a smaller area to operate. To adjust to these two unequal forcings, the fluid parcel moves slowly as it leaves the convection region in the northeast, being very gradually warmed along its anticyclonic course. As it reaches the western boundary, it turns to move north, enters the convection region and must *speed up* for all the heat accumulated along the slow anticyclonic journey is flushed upward extremely quickly by convection. It is therefore both the very unequal efficiency of heat loss and heat gain mechanisms and the anticyclonic flow path of the upper layers which lead to the f plane western intensification (eastern intensification would occur with a surface cyclonic flow). The effect relies on the importance of the horizontal nonlinear terms and operates most efficiently near the surface where the flow speeds and temperature gradients are largest. As can be seen (Fig. 19) the zonal asymmetry indeed disappears in the deeper layers. As is shown in the next section, the buoyancy driven circulations are extremely sensitive to the vertical mixing coefficient increasing their strengths with it. To test the soundess of the above reasoning a run with a higher vertical mixing (K_v = 5 cm^2 s^{-1}) was carried out. It revealed that indeed the western intensification was larger, indicating the importance of horizontal transport terms in the argument. There is of course no reason to expect that the process here exposed should not operate in the more realistic β plane case discussed earlier and it may be suggested that the western intensification is reinforced in such cases by the necessary increase of the positive horizontal heat transport to feed the active heat loss regions to the north. In the abyss, however, it is clear that the western intensification is due to β alone.

9. The small amplitude limit

A useful limit to look into is the small amplitude case obtained when the forcing is gradually decreased. With a uniform atmospheric temperature gradient imposed at the surface, a decrease of the strength of the gradient weakens advection effects and interior horizontal divergence. This transition pictured in Figure 20 shows increasingly zonal flows as the forcing amplitude decreases. The planetary vorticity balance requires these zonal flows when the interior vortex stretching becomes small. In the meantime the heat transport is carried increasingly by lateral diffusion. It is however at very small forcing levels (less than 0.1°C per 1000 km) that the ratio of advective to diffusive fluxes becomes less than 50%. The response to these very low forcing levels is described below. The first point is that the spin up times are much longer than in the nonlinear case: typically one must integrate for at least 1500 years to obtain an approximate energy balance between convection and vertical mixing. This is because it takes a full diffusive time scale for the largest scale to get steady and it is these largest

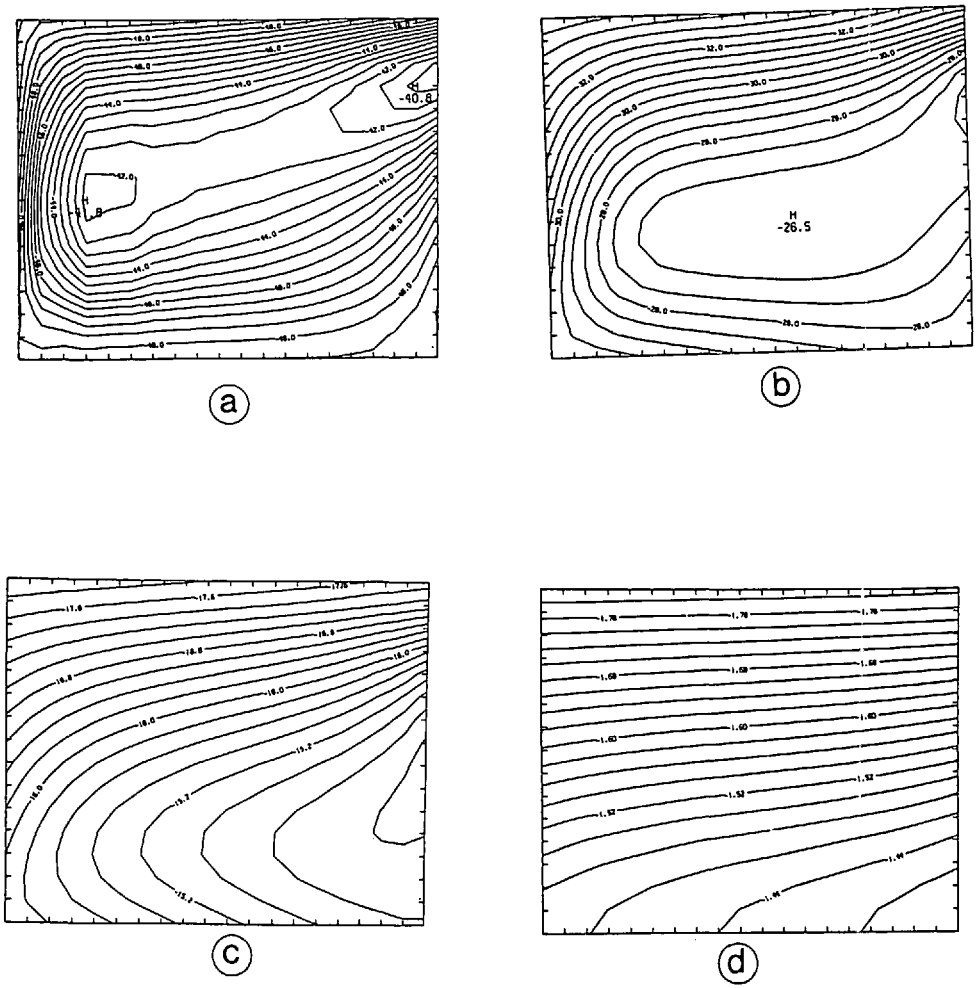

Figure 20. The pressure fields at 475 m for several imposed atmospheric temperature gradients. (a) 1.9°C per 1000 km, (b) 0.4°C per 1000 km, (c) 0.1°C per 1000 km, (d) 0.01°C per 1000 km. As the gradient decreases, the meridional circulation weakens.

scales which contribute most to the global heat transport. After such a spin-up the surface buoyancy forcing and northern convection regions are uniform zonally. The temperature fields (Fig. 21) reveal that the concept of a thermocline disappears. Instead the thermal field varies over a depth scale of the order of the ocean depth, a fact consistent with the long sign-up times. A purely diffusive balance would predict a vertical scale $L(K_v/K_H)^{1/2}$ or about 2 km with the parameters used. This is perhaps the clearest sign that the existence of an oceanic thermocline has a nonlinear origin. The broad temperature and pressure patterns are quasizonal at all depths. The powerful recirculations of the large amplitude case and the western intensification are absent.

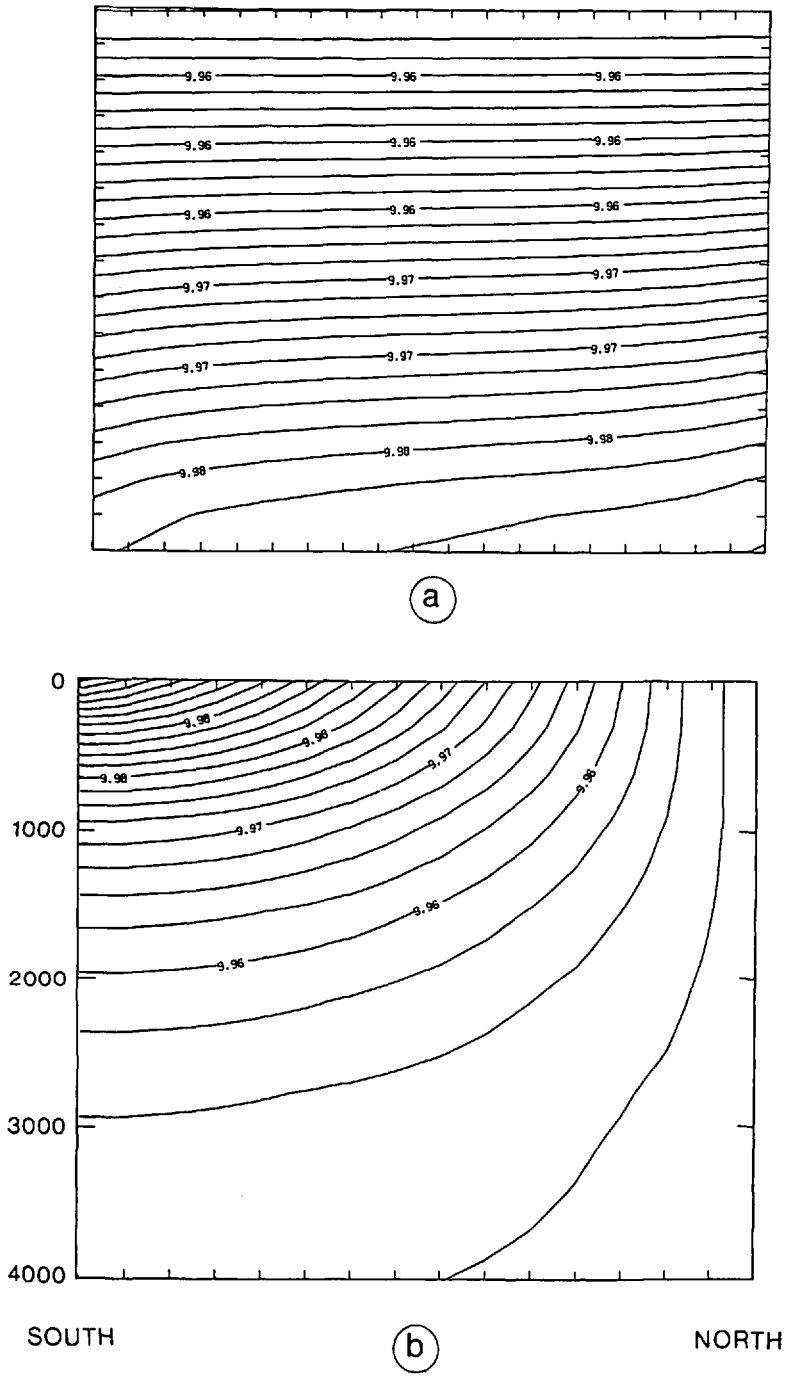

Figure 21. The temperature field when the atmospheric temperature gradient is 0.01°C per 1000 kms; (a) horizontal map at 475 m, (b) vertical meridional section in the eastern basin field. Note the very different aspect ratio of the thermocline comparing with the finite amplitude thermocline of Figure 7.

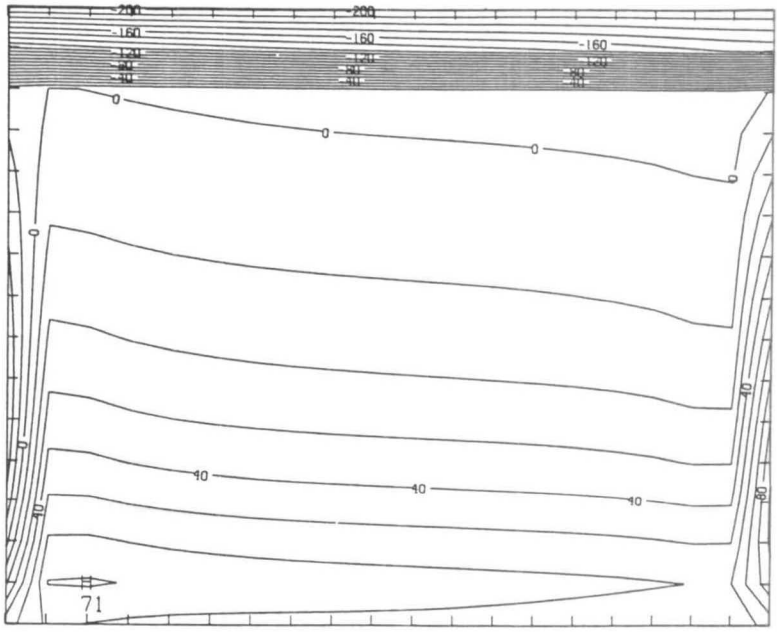

Figure 22. The horizontal Laplacian of the temperature field of the small amplitude solution shown in Figure 21 (a): 3 regimes can be identified. Horizontal diffusion is balanced by convection in the northern region, by vertical mixing in the interior and by vertical advection along meridional boundaries.

The advective field is made of a broad eastward flow above 1500 m with westward flow below. Even at such low forcing levels a discernable north-south component is also present and gives to the circulation the sense of a Hadley cell albeit strongly tilted in the zonal direction. This cell does not account for more than 5% of the needed meridional transport. It has negligible negative interior vertical velocities, vertical communication occurring through thin (one grid point wide) boundary layers with upwelling (downwelling) distributed along the western (eastern) boundary. At the vorticity equation level the associated vortex stretching is balanced by lateral diffusion in these layers. Even with such a simple thermal structure, the heat balance of terms shows several regimes. The central term which redistributes the heat meridionally is the lateral diffusion term shown in Figure 22. Within regions of heat gains it is balanced by vertical diffusion and by convection in regions of heat losses. Such balances dictate the distribution of the meridional temperature gradient consistent with a northward heat transport. It must be maximum south of the convection region decreasing to smaller values on either side. Of more interest is the structure at the western and eastern walls. In these two regions vertical advection is important to balance lateral diffusion. Even at such small amplitude levels (interior horizontal velocities are order 0.1 mm s^{-1} when the applied gradient is 0.01°C over 1000 km) the

vertical advection terms are not negligible everywhere. The sources and sinks of mass distributed along the meridional boundaries induce heat sources and sinks at each level: the solution is not determined uniquely by a 3 dimensional Poisson type equation. At each level vertical advective heat transport along the side wall occurs and the solution remains intrinsically nonlinear. The very nature of these side wall layers is probably the greatest difficulty to formulate theoretical solutions of buoyancy driven flows in bounded domains. Salmon (1986) discusses such limits by linearization of the vertical advection terms around a state of flat isopycnals given *a priori*. The diffusive limit has also been examined analytically by Rattray and Welander (1975) with solutions looking qualitatively as the present numerical ones. The domain of validity of their solution is however more restricted than indicated in their study. For the vertical advection term to be negligible in the sidewall boundary layer it is required that:

$$w\rho_z \ll K_H \rho_{yy}.$$

In the boundary layer w_z is $O(u_x)$ and the width of the boundary layer needed to bring horizontal velocities to zero at the wall is $O(A_H/f)^{1/2}$ when lateral friction is invoked. Scaling the above inequality with that lateral scale yields:

$$\frac{UL}{K_H} \ll \left(\frac{A_H}{f_o L^2}\right)^{1/2}$$

i.e., the horizontal Peclet number must be much less than the squareroot of the horizontal Ekman number itself much less than one. This restriction does not appear to have been noticed by Rattray and Welander who go up to order one Peclet numbers to illustrate their solutions. For the above inequality to be satisfied with the parameters of the numerical solutions discussed herein, the horizontal Peclet number must be much less than 10^{-2}, the horizontal velocities much less than 10^{-4} cm s^{-1} and the external temperature gradient much less than 10^{-5}°C per 1000 km. This lack of realism of the linear solution is problematic: even though the interior may be assumed linear the full 3D stratification is influenced by the nonlinear character of the sidewall layers for all reasonable amplitudes of the motions.

10. Parameter sensitivity

This last section is provided to ascertain the relevance and robustness of the previous solution and to study its sensitivity to unresolved nonadiabatic processes. The most novel study would be to try different parameterization of vertical transport processes in both stratified and unstratified regions; however we shall content ourselves to vary the value of the diffusive coefficients around some pivot value. For the sake of economy we use a lower resolution version of the model (slightly more frictional and diffusive) than the one discussed at length previously (Table 1). The range of parameter values explored at low resolution is meant to test the stability of certain features of the

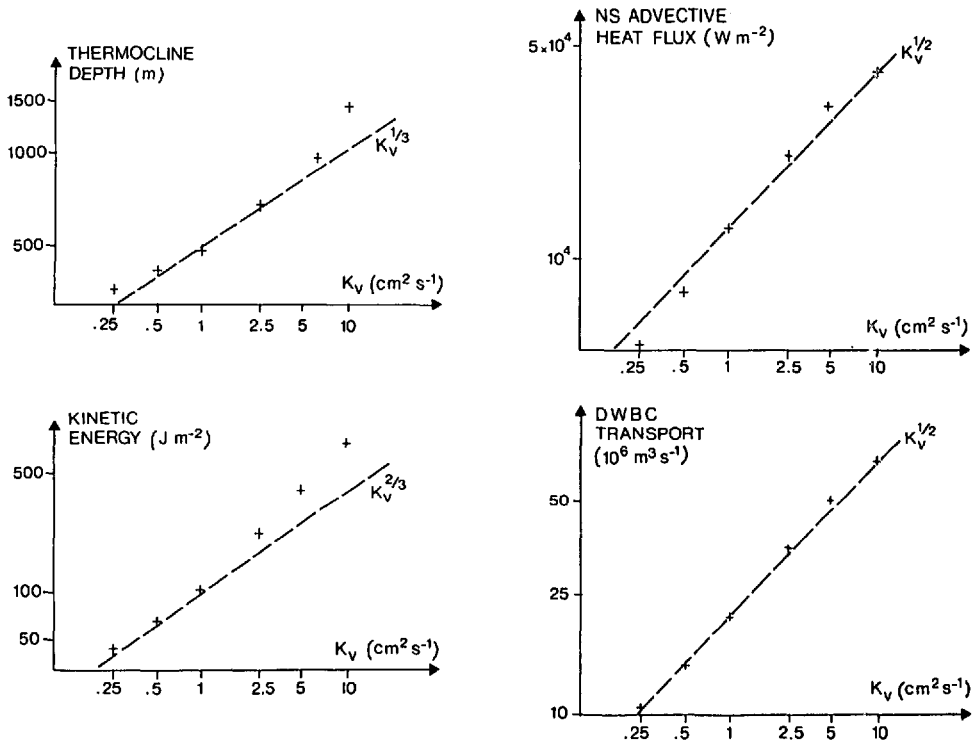

Figure 23. Mean thermocline depth, NS advective heat flux, kinetic energy and deep western boundary current as a function of the vertical mixing coefficient K_v.

previous solution and to show quantitatively the variation of certain integrated quantities such as meridional heat flux.

a. Vertical mixing. Variations of advective meridional heat flux, kinetic energy, depth of the thermocline and deep WBC transport are shown as a function of K_v on Figure 23. All these quantities increase with the vertical mixing coefficient revealing a great sensitivity to that parameter a fact already noticed by Bryan (1986) within the GFDL primitive equation model. If one compares oceanic estimates of deep WBC transport or meridional heat flux with the model results, a choice of a value of K_v around unity would appear to be the most sensible. As discussed previously the heat equilibrium which shapes the subtropical interior circulation is one of balance between vertical advection and vertical mixing in the main thermocline. As the vertical mixing increases, downward heat penetration increases and the heat transport must also increase in a steady state. It does so by speeding up the flow since the temperature gradient is imposed externally in this problem. Therefore the direct Hadley cell which redistributes heat in the meridional plane becomes more intense along with the convection to the north. Following Welander (1971) a scaling law may be deduced

from such a reasoning. The depth D of the thermocline is obtained from the heat balance in the thermocline:

$$D \simeq K_v/W.$$

Furthermore interior vorticity balance gives:

$$U \simeq R_E/DW$$

where R_E is the earth radius. Finally given an imposed external gradient $\Delta\rho/L$, the thermal wind yields:

$$fU \simeq g\, D\Delta\rho/\rho_o L.$$

Eliminating U and W in these 3 relations gives:

$$D \simeq \left[K_v \frac{R_E L f}{g\Delta\rho/\rho_o}\right]^{1/3}$$

The thermocline depth varies therefore as $K_v^{1/3}$, the interior vertical velocity as $K_v^{2/3}$ and the horizontal velocity as $K_v^{1/3}$. These laws indicated in Figure 23 show the horizontal kinetic energy and thermocline depth scale approximately as above, revealing a sensitivity somewhat greater. It demonstrates that the above scaling which underlies the previous discussions, is associated with one of the dominant regimes of the model circulation. Meridional advective heat flux and deep WBC transport appear to be more sensitive to K_v increasing as its squareroot.

Key features of the pivot circulation have already been identified and it is useful to see qualitatively how they are influenced by K_v. An increase of the latter has the following results:

—The vertical penetration of the upper anticyclonic gyre increases. The northward flowing Gulf Stream extends deeper.

—The convection region increases in size to the south and penetrates deeper.

—The deep eastern boundary current between the mid-thermocline level and the bottom disappears.

—The deep cyclonic gyre intensifies to the north: the direct meridional flow from the deep water source to the DWBC region increases and the index of horizontal recirculation decreases.

With K_v equal to 0.25 cm^2 s^{-1} (much below the pivot value), the meridional circulation becomes weak as does the convection which does not reach the bottom. At the same time, mass sinking is prevented from reaching the deepest layers and a reverse cell appears. However at such low values, the spin up of the model is hard to achieve and it is possible that a numerical problem as noted in Bryan *et al.* (1974) appears with the development of a computational mode in the vertical direction. More vertical resolution is called for but such runs become expensive for the spin up times become large as well.

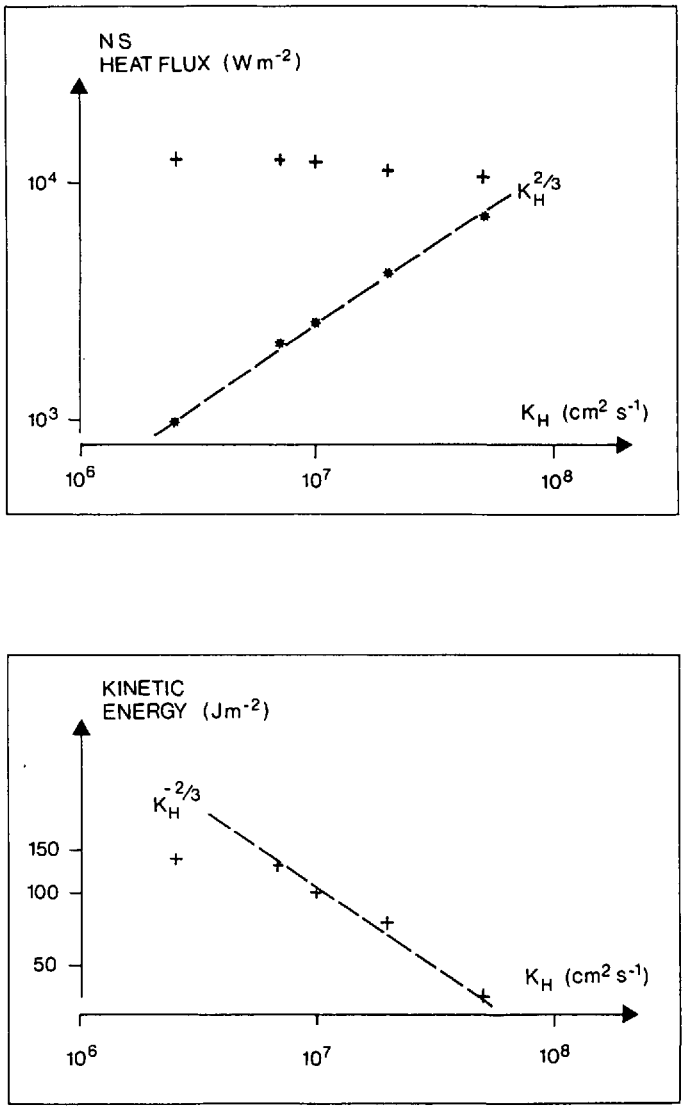

Figure 24. NS heat flux (+ advective, * diffusive) and kinetic energy as a function of the horizontal mixing coefficient K_H.

b. Horizontal diffusion. Integrated quantities are presented in Figure 24 when K_H varies from 2.5 10^6 to 5 10^7 cm^2 s^{-1}. The advective heat fluxes are rather insensitive to K_H while the diffusive ones increase rather precisely as $K_H^{2/3}$. At the upper end of the range of K_H, advective and diffusive fluxes become of comparable magnitude, the former dominating in the south, the latter in the north. The effect of horizontal diffusion is far more important on the kinetic energy which increases by a factor of 4 over the range explored, the meridional heat flux and the rate of bottom water

formation hardly varying by no more than 10%. Lateral diffusion bears mostly on that part of the flow recirculating in the horizontal plane but has little influence on the vertical Hadley cell responsible for the heat transport. Other features sensitive to K_H are:

—the western boundary current which of course broadens with K_H,

—the mid-depth abyssal eastern boundary current which disappears with increasing K_H.

Therefore the boundary layer width of these features depends on K_H since the frictional dissipation was held constant in these runs. If we replace velocity by its geostrophic value in Eq. (11), a balance between horizontal density diffusion and the β term leads to a boundary scale K_H/C exceeding the Munk layer width for sufficiently large K_H (C is the internal Rossby wave speed).

It is clear that this exploration is far from complete but demonstrates the following: the overturning circulation in the vertical meridional plane increases with K_v at the expense of horizontal recirculation which on the contrary responds to lower K_H values. As a result the meridional heat fluxes are very sensitive to K_v but not to K_H. The subthermocline eastern boundary current of the pivot solution depend on both K_v and K_H and weakens as either one increases above the pivot value.

Acknowledgments. I started working on this problem while enjoying a sabbatical leave at NCAR. I wish to thank more specially P. Gent, J. McWilliams and P. Schwartztrauber whose conversations were extremely useful in the early stages of construction of the numerical model. The help of G. Veronis to improve the manuscript is gratefully acknowledged. Computations were carried out at CCVR (Palaiseau, France). The NCAR graphic package was used repeatedly.

APPENDIX

Numerical methods

The 3 dimensional grid used to discretize the set of equations (10) obeyed by the baroclinic mode is shown in Figure A1. The vertical grid is classical and was proposed by Lorenz (1960), as a way to preserve quadratic invariants in the advection equation. The vertical velocity w is carried at odd levels while u, v, p, ρ are evaluated at even levels.

In the horizontal plane u, v, p, ρ, w are carried at each grid point, while the no slip condition is applied half a grid point away from the nearest interior grid point. Other staggered grids are commonly used in primitive equation models: the present choice is motivated by the form of the friction terms required by the energy conservation law. Introducing the notation:

$$\delta_x \Phi = \frac{\Phi_{i+1/2} - \Phi_{i-1/2}}{\Delta x}, \quad \delta_z \Phi = \frac{\Phi_{k-1/2} - \Phi_{k+1/2}}{Z_{k-1/2} - Z_{k+1/2}}$$

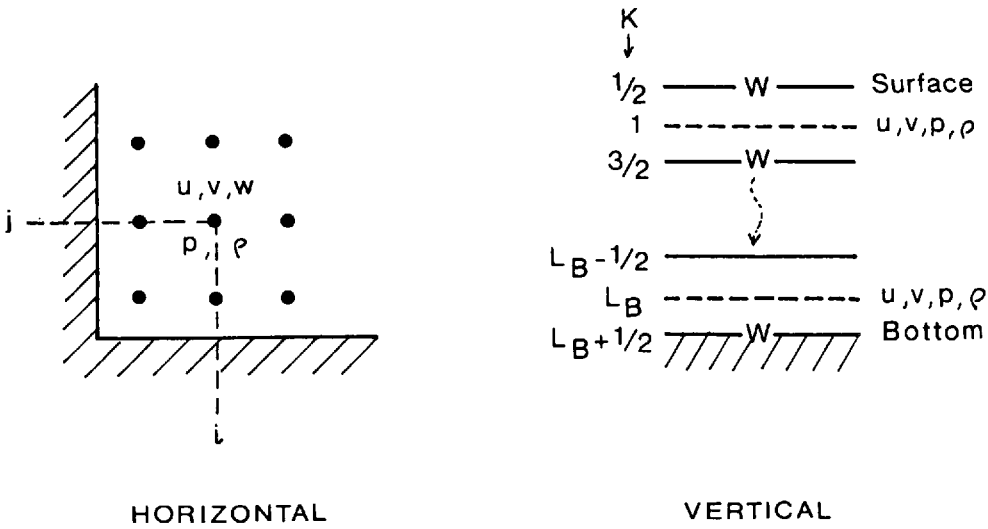

Figure A1. Horizontal and vertical grids of the model.

and

$$\overline{\Phi}^x = 1/2\,(\Phi_{i+1/2} + \Phi_{i-1/2})$$

the discrete set of equations (10) (less the forcing terms) can be evaluated at the generic point i, j, k (i zonal, j meridional, k vertical index):

$$-fv = -\overline{\delta_x P}^x/\rho_o + A[\delta_x(\delta_x u) + \delta_y(\delta_y u)]$$

$$+fu = -\overline{\delta_y P}^y/\rho_o + A[\delta_x(\delta_x v) + \delta_y(\delta_y v)]$$

$$\overline{\delta_x u}^x + \overline{\delta_y v}^y + \delta_v w = 0 \qquad \text{(A1)}$$

$$\delta_z P + g\overline{\rho}^{zz} = 0 \text{ (or } \delta_z P + g\overline{\rho}^z = 0 \text{ evaluated at } k + 1/2)$$

$$\partial\rho/\partial t + \delta_x(\overline{u}^x\overline{\rho}^x) + \delta_y(\overline{v}^y\overline{\rho}^y) + \delta_z(w\overline{\rho}^z) = K_v(\delta_z\delta_z\rho) + K_H(\delta_x\delta_x\rho + \delta_y\delta_y\rho)$$

with BC$_z$: $u = v = 0$ at $i = -1/2, i = M - 1/2$

and $j = -N + 1/2$ and $j = N + 1/2$

and $w = 0$ at $k = -1/2$ and $k = L_B + 1/2$.

The centered differences apparent in A1 give a $0(\Delta x^2)$ truncation error. To derive conservation laws a number of relations easy to check are useful:

$$\varphi\delta_x\Psi = \delta_x(\overline{\varphi}\Psi^x) - \overline{\Psi\delta_x\varphi}^x$$

$$\overline{\varphi}^x\delta_x\varphi = \delta_x(\varphi^2/2)$$

$$u\overline{g}^x - \overline{\overline{u}^x g}^x = -\Delta(x^2/4)\delta_x(g\delta_x u)$$

$$\sum_{i=0}^{M-1}\delta_x\overline{g}^x = \overline{g}^x_{M-1/2} - \overline{g}^x_{-1/2}$$

Multiplying the density equation by gz_k, the momentum equations by the velocity vector $\boldsymbol{u}$, adding the result and summing over i, j, k yields:

$$\sum_{ijk} \frac{\partial \rho_{ijk}}{\partial t} g z_k \Delta x_i \Delta y_j \Delta z_k$$

$$= -A \sum_{ijk} \overline{[(\delta_x u)^2]}^x + \overline{[(\delta_y u)^2]}^y + \overline{[(\delta_x v)^2]}^x + \overline{[(\delta_y v)^2]}^y \Delta x_i \Delta y_j \Delta z_k$$

$$+ K_v \sum_{ij} [\rho_{ij\,bot} - \rho_{ij\,surf}] \Delta x \Delta y.$$

The finite difference form of the energy equation is therefore completely equivalent with the continuous form (7) and there are no fictitious terms introduced by the discretization. It is also not difficult to prove that the advective terms in the density equation are such that the volume integral of both ρ and ρ^2 are conserved under adiabatic conditions. These kind of invariants are extremely useful for the stability properties of the scheme and as guidelines in the actual coding of the model. The time differencing scheme is the Matsuno's predictor-corrector. Knowing ρ at step n one first computes ρ^* as:

$$(\rho^* - \rho^n)/\Delta t = F(\rho^n)$$

and then ρ^{n+1} as:

$$(\rho^{n+1} - \rho^n)/\Delta t = F(\rho^*).$$

The truncation error is $0(\Delta t)$ and the scheme has the same stability conditions as explicit methods. In such a multistep method the computational burden is doubled. The Matsuno scheme has artificial diffusion for the transient case which decreases linearly with Δt and has *no artificial diffusion in the steady state.* This is very desirable as the emphasis of the simulations is precisely on such steady states. Early experiments with less costly leap-frog time stepping showed that stability required a very stringent condition ($A\Delta t/\Delta x^2 \leq 1/8$) limiting far too severely the time step. Under the FD form of the equations (A1) the only outstanding problem to be solved lies with the momentum equations. Given the pressure gradient two coupled Helmhotz equations with small friction coefficients must be solved. This singular elliptic problem is handled by direct methods. A Fourier transform is performed in the zonal direction using quarter wave transform adapted to the staggered boundaries (see Schwartzhauber (1982) for information about such Fourier transforms). The pentadiagonal system which remains in the meridional direction is solved by Gaussian elimination with partial pivoting using a standard Linpack routine.

A number of accuracy checks have been carried out initializing the model with a random distribution of density values. The linear invariants density and potential energy are conserved with machine accuracy while the quadratic density variance is conserved with an accuracy proportional to Δt as it should be with a first order scheme

in time. Simple Rossby wave solutions were also tested and compared against theoretical solutions. Finally stability boundaries were sought empirically varying one parameter at a time. The stability criterions are the following:

$$U\Delta t/\Delta x \leq 0.5$$
$$C\Delta t/\Delta x \leq 310^{-2}$$

(where C is the first baroclinic Rossby mode speed)

$$K_H\Delta t/\Delta x^2 \leq 1/8.$$

The first two criteria are the more stringent ones in the parameter range used. The second one in particular is surprising and dominant in a linear problem. When the criterion is not met, a boundary type instability develops first at the southern boundary. Fortunately the baroclinic Rossby waves are slow and the constraint is not too damaging. Finally the model running on a Cray-1 takes about 24 microseconds per time step and grid point (remember that this is a 2 step method). As an example a 1000 year simulation using the low resolution choice ($20 \times 16 \times 8$) can be run with a week time step and takes under one hour of computer time. The particular vertical discretization and initial stratification chosen for all runs presented herein is the following:

Thickness of vertical layers (m)	100	250	250	400	500	500	1000	1000
Vertical layers position (m)	50	225	475	800	1250	1750	2500	3500
Initial temperature stratification (Celsius)	15	12	10	6.2	4.5	3.5	3.5	3.5

REFERENCES

Bryan, F. 1986. On the parameter sensitivity of primitive equation ocean general circulation models (submitted).

Bryan, K. and M. D. Cox. 1968. A non-linear model of an ocean driven by wind and differential heating: Part I—Description of the three dimensional velocity and density fields. J. Atmos. Sci., *25*, 945–967.

—— 1984. A numerical model of the ventilated thermocline. J. Phys. Oceanogr., *4*, 674–687.

Bryan, K., S. Manabe and R. C. Pacanowski. 1974. A global ocean-atmosphere climate model. Part II: The oceanic circulation. J. Phys. Oceanogr., *5*, 30–46.

Bunker, A.F. 1976. Computations of surface energy flux and annual air-sea interaction cycles of the North Atlantic. Mon. Weather Rev., *104*, 1122–1140.

Charney, J. 1975. Discussion p . . . , *in* Numerical Models of Ocean Circulation. Nat. Acad. Science, Washington, DC.

Colin de Verdière, A. 1986. On mean flow instabilities within the planetary geostrophic equations. J. Phys. Oceanogr., *16*, 1981–1984.

Freeland, H. J., P. B. Rhines and T. Rossby. 1975. Statistical observations of the trajectories of neutrally buoyant floats in the North Atlantic. J. Mar. Res., *33*, 383–404.

Gent, P. and J. McWilliams. 1983. Regimes of validity for balanced models. Dyn. Atm. Oceans, *7*, 167–183.

Haney, R. L. 1971. Surface thermal boundary condition for ocean circulation models. J. Phys. Oceanogr., *16*, 241–248.

Hasselman, K. 1982. An ocean model for climate variability studies. Prog. Oceanogr., *11*, 69–92.

Hogg, N. 1983. A note on the deep circulation of the western North Atlantic: its nature and causes. Deep-Sea Res., *30*, 945–961.

Holland, W. 1971. Ocean tracer distributions—a preliminary numerical experiment. Tellus, *23*, 371–392.

Lorenz, E. N. 1960. Energy and numerical weather prediction. Tellus, *12*, 364–373.

Luyten, J. R., J. Pedlosky and H. Stommel. 1983. The ventilated thermocline. J. Phys. Oceanogr., *13*, 292–309.

McCartney, M. S. and L. D. Talley. 1982. Distribution and circulation of Labrador Sea Water. J. Phys. Oceanogr., *12*, 1189–1205.

Munk, W. H. 1966. Abyssal recipes. Deep-Sea Res., *13*, 707–730.

Pedlosky, J. 1979. Geophysical Fluid Dynamics. Springer-Verlag.

Phillips, N. A. 1963. Geostrophic motion. Rev. Geophys. Space Phys., *1*, 123–176.

Rattray, M. and P. Welander. 1975. A quasilinear model of the combined wind driven and thermohaline circulation in a rectangular β plane ocean. J. Phys. Oceanogr., *5*, 585–602.

Rhines, P. B. and W. R. Young. 1982. Homogenization of potential vorticity in planetary gyres. J. Fluid. Mech., *122*, 347–367.

—— 1982. A theory of wind-driven ocean circulation. I—Mid ocean gyres. J. Mar. Res., *40* (Supp.), 559–596.

Richardson, P. 1977. On the crossover between Gulf Stream and western boundary undercurrent. Deep-Sea Res., *24*, 139–159.

—— 1985. Average velocity and transport of the Gulf Stream near 55N. J. Mar. Res., *43*, 83–111.

Robinson A. R. and H. Stommel. 1959. The oceanic thermocline and the associated thermocline circulation. Tellus, *3*, 295–308.

Roemich, D. 1980. Estimation of meridional heat flux in the North Atlantic by inverse methods. J. Phys Oceanogr., *10*, 1972–1983.

Salmon, R. 1986. A simplified linear ocean circulation theory. J. Mar. Res., *44*, 695–711.

Schwarztrauber, P. N. 1982. Vectorizing the FFT's in Parallel Computations. Academic Press.

Stommel, H. 1948. The westward intensification of wind driven ocean currents. Transactions AGV, *29*, 202–206.

Stommel, H. and A. B. Arons. 1960. On the abyssal circulation of the world ocean. II—An idealized model of the circulation pattern and amplitude in oceanic basins. Deep-Sea Res., *6*, 217–233.

Veronis, G. 1969. On theoretical models of the thermocline circulation. Deep-Sea Res., *16*, (Suppl.) 301–323.

—— 1975. The role of models in tracer studies. Symposium on Numerical Methods in Oceanography. National Academy of Sciences, 133–146.

Welander, P. 1971. The thermocline problem. Phil. Trans. Roy. Soc. Lond., A. *270*, 415–421.

Received: *27 July, 1987;* revised: *27 December, 1987.*